STUDY AND APPLICATION OF SOFT COMPUTING TECHNIQUES FOR HOTSPOT MONITORING USING SATELLITE DATA

A DISSERTATION

Submitted in partial fulfillment of the requirements for the award of the degree
of
MASTER OF TECHNOLOGY
in
DISASTER MITIGATION AND MANAGEMENT

By

JOWHERALI SYED MOHAMED JASHIM

CENTRE OF EXCELLENCE IN DISASTER MITIGATION AND MANAGEMENT
INDIAN INSTITUTE OF TECHNOLOGY ROORKEE
ROORKEE-247667 (INDIA)

MAY, 2016

CANDIDATE'S DECLARATION

I hereby certify that work presented in the Dissertation titled "**Study and Application of Soft Computing Techniques for Hotspot Monitoring using Satellite Data**" in partial fulfillment of the requirement for the award of **Master of Technology in Disaster Mitigation and Management** in the Centre of Excellence in Disaster Mitigation and Management (CoEDMM), Indian Institute of Technology Roorkee, is an authentic record of my own work carried out during the period from July 2014 to May 2016 under the supervision and guidance of **Dr. Dharmendra Singh**, Professor, ECE, Indian Institute of Technology Roorkee, Uttrakhand, India.

The matter presented in this Dissertation has not been submitted by me for the award of any other degree.

Date: 26/5/2016

Place: Roorkee

JOWHERALI SYED MOHAMED JASHIM

(Enrolment No. 14552003)

CERTIFICATE

This is to certify that the work contained in the above statement made by the candidate is correct to the best of my knowledge.

26/5/16

Prof. Dharmendra Singh
Department of Electronics and Communication Engineering
IIT Roorkee
UK-247667, India

ACKNOWLEDGEMENT

It gives me great pleasure to take this opportunity to thank my guide Dr. Dharmendra Singh, my supervisor, for his invaluable discussions, suggestions, and guidance despite his very busy schedule. Throughout the entire duration of this thesis, he has been an inspiration to me. His help always extended to me, whenever I needed. The help rendered by him is invaluable and unforgettable. He has constantly guided me academically and always inspired me over improving my thought process about how to approach a problem and solve it efficiently. Have been a mentor who gave encouragement and instill motivation and gave a lot of encouragement to think creatively and develop an attitude of learning as much as one can. My earnest thanks to Dr. Dharmendra Singh for providing me a quad in his research lab with an ideal research environment.

I am indescribably happy to place my sincere gratitude to Chairman-CAPC Dr. Kamal Jain as well as to the Head of Department Dr. B.K. Maheswari for their support and encouragement over sharpening my personality.

I also extend my gratitude to all my lab partners for their valuable support. I would like to especially thank Dr.Tasneem, Mr.Deepak, Mrs. Akansha and the list is endless for the valuable suggestions without which it would have been very difficult. I would like to thank my friends Avanish Mishra, Rohit and Abhay for all those petite chats during stressful conditions.

I am indebted to the Ministry of Human Resource Development (MHRD), Govt. of India for providing me financial support during my research work as well as to DST-INRIA for providing me material support during my thesis work.

My Heartfelt thanks to my parents and brothers for their support and their uphill encouragement throughout my life and to my pal Sudhan Nair "a brother from another mother".

ABSTRACT

The aim of the dissertation is to elaborate the remote sensing methods for monitoring subsurface fire (hotspots) in Jharia Region, (Jharkhand) India; as the Jharia coal field contains almost half of subsurface mine fires within the Indian coal fields [1]. Thus, detecting and monitoring such hotspots are mandatory. Since ground based monitoring are quite expensive and difficult task, exploiting the potential of satellite images have been tried as an alternative solution. For this purpose, freely available satellite images (e.g., MODIS, NOAA/AVHRR, and LANDSAT) are being used for our study. This study involves the application of most renowned soft computing techniques such as: supervised classification (parallelepiped, minimum distance) and unsupervised classification (ISODATA, K-means) over optical data: MODIS, NOAA/AVHRR, and LANDSAT. NDVI plays an important role for the detection of hotspot due to the fact that hotspot region usually has bare ground such that neither bushes nor grasses grows over hotspot region. Thus, NDVI classified image into hotspot and non-hotspot regions is used. The accuracy of the classified image is assessed using the metrics: hotspot detection accuracy (HDA) and false alarm rate (FAR). The assessed value indicates that there is room for improvement. Thus, an attempt based on heuristic method- genetic algorithm (GA) have been carried out, since it has higher chances to result in an optimal classification of hotspot and non-hotspot pixels due to its ability to search for the optimal hypothesis over a larger search space. Therefore, the attempt of GA based KMI (K-Means Index) indicates that the detection of hotspot with an accuracy of 81%-HDA and 11%-FAR over MODIS dataset.

Such high HDA and low FAR over detection of hotspot and an attainment of good temporal resolution recommends use of MODIS dataset for area estimation over hotspot coverage in Jharia region. But due to fragment size of hotspot in comparison to spatial resolution of MODIS, major amount of hotspot are present partially within a pixel (i.e., mixed pixel issues). In order to perform hotspot area estimation over such coarse resolution image, subpixel analysis is performed; by refining the per-pixel spectral-based detected hotspot from MODIS image by

proposing a method that uses a subpixel spectral detection method called CEM (a target constraint approach). Constrained energy minimization (CEM) is very efficient in the detection of small hotspots very effectively as well as it requires only a prior knowledge of target spectral signature. Due to the requirement of hotspot pure spectral signature, we have used LANDSAT-5TM image for the endmember selection using PPI. With such refined detected hotspots, the estimated area coverage of hotspot were found to be of 11.09 Km^2 (on 14-Mar-2015) and when validated with week and yearly variation; it is observed that hotspot of 0.165 Km^2 of variation been observed within two weeks interval and 2.647 Km^2 of increased Hotspot coverage is observed over a period of two years.

Table of Contents:

LIST OF FIGURES:

LIST OF TABLES:

CHAPTER 1

INTRODUCTION

Satellites have led to obtain variety of information about the earth's surface, which are ranging from predicting weather patterns globally, monitoring surface vegetation, tectonic activities, polar ice variation, pollution, and variation in temperature scales, cloud cover and many more applications.

Satellites have played a vital role in obtaining valuable information about the earth surface which led to have a better understanding over the changes occurring within our environment such as: predicting weather condition, monitoring surface vegetation,

Images obtained from satellites are the best source to obtain details about the resource coverage of a region which could be used for resource management in an efficient way. Resources include mineral, forest, agricultural, forest, hydrological, geological resources etc. These information are obtained/extracted from the satellite images using digital image processing.

The reduction in price of the satellite images for the availability among the public and the abundant availability of satellite images of various resolution has lead to the involvement of researchers among various countries to be involved to bring an evolution of gathering information about the earth resource without in physical contact to the target (eg: land surface) and occurring and sharing such information throughout the globe in least amount of time.

The satellite images can be distinguished based on different spatial resolution and spectral characteristics. Resolution is the characteristic of an image that describes the level of detail that can be distinguished. Since the smallest unit in the satellite image is a single pixel, thus a minimal scale of the earth surface that can be extracted from the image is equivalent to the size of a single pixel. Major satellite images are available with the spatial resolution of about 50 centimeters to 100 meters. Based on the resolution of an image the usage of the image can be varied. The high resolution satellite data such as IKONOS, QuickBird, ASTER which offers spatial resolution up to 60 centimeters whereas low resolution data such as NOAA/AVHRR and MODIS provides the spatial resolution of 1.1 km and (250-1000 meters) but due to the advantage

of higher temporal resolution (i.e., several times coverage of a region in a day); these low resolution data can be used in applications such as forest fire monitoring, drought and flood occurrence etc which covers huge land area. Thus, due to the higher revisit of a region and the free available of such low resolution data has led to wider involvement of researchers to find techniques that results in extract of finer details from such coarse spatial resolution images. Also, the high resolution images can be used for various purposes but the major issue is the less availability of images at different intervals of time and limited spatial coverage has put a limitation towards the usage of high resolution satellite data.

Day by Day the world is facing various geographical and environmental crisis for which satellite images can be used as an effective source of remedy to mitigate such issues. Among these problems, the problem occurred due to subsurface coal fires (further on will be called as hotspots) is a problem to be prioritized in coal producing countries. The coal fires can cause severe damages to the environment such as: air pollution, land cracks and subsidence, deposition of unwanted/toxic chemicals over land leads to invalid use of land covers, emission of smokes can lead to lung related diseases. These can disturb the entire ecosystem by releasing toxic fumes, greenhouse gases. It also affects human health as the people in such affected areas are found to suffer from various diseases like tuberculosis, asthma; majority of population could suffer from breath related diseases.

As per today, there are plenty of methods are suggested by the researchers to use satellite data to analyze and detect coal fires. In order to bring out a better accuracy among such detection, techniques of soft computing could be utilized as the uncertainty among the detection (i.e classification) of hotspots could be resolved to a better approximate as the soft computing techniques are widely known to resolve such issues.

Natural resources are the backbone of the economy. Mining of these natural resources is carried out worldwide. However, various hazards are triggered due to mining of natural resources. One such natural resource is coal, which is a non-renewable source of energy. Mining of coal is carried out for centuries because of its numerous benefits such as source of fuel, electricity etc. Hazards associated to coal mining are for example, land subsidence, surface and subsurface coal-fires.

Some of the very noticeable affects due to coal fire are [1]:

- Land subsidence.
- Emission of large quantity of toxic and greenhouse gases such as: SO_2, NO, CO, CH_4 and CO_2 resulting in pollution of environments and adversely affects the health of millions of people.
- Land deformations occurred due to the activity of underground coal fires affects the human settlements.
- Due to unwanted and uncontrollable burning of valuable coal deposits results in major economic loss.

Thus, for the sustainable development of the mining environment, the socio-economic impacts, environmental impacts, health and safety issues of the local people results in firm need of an effective mitigation measures.

1.1 Soft computing

Soft computing is the use of approximate solutions to solve computationally hard problems (ie., those problems that cannot be solved in polynomial time) such as NP-Complete problems. As they resemble natural processes more closely than traditional techniques, which are majorly dependent on formal logical systems, such as sentential logic and predicate logic, or rely heavily on computer-aided numerical analysis (as in finite element analysis). In short, they have similar computation as found in human mind.

Soft computing are majorly used in many modules (preprocessing module, enhancement module) in remote sensing but majorly involved in classification of satellite Images.

1.1.1 Goals of soft computing

- It is a new multi-disciplinary field which is applied to construct new generation Artificial Intelligence system whose functionality are almost an emulation of computational neuroscience.
- The main goal of soft computing is to provide solutions to real world problems, which cannot be modeled or too difficult to model mathematically.

- Task –II:

  Application of subpixel analysis for area estimation of hotspot coverage using constrained target subpixel detection method.

1.3 Organization of thesis

The report is organized as follows. Chapter 2 provides an overall survey of various literatures in correspondence to the application of soft computing techniques over satellite images majorly focusing over detection of coal fires as well as over the various subpixel classification techniques.

In Chapter 3 the types of satellite images is briefly written while highlighting the advantages of NDVI index over the satellite images in regards to utilize it for our purpose. Also, it includes theoretical background about various soft computing techniques over image classification as well as elaboration about methods used for performing subpixel classification using constrained target approach, a description on PPI for endmember extraction and brief overview on segmentation especially on Otsu method and segmentation as clustering problem using cluster a well-known similarity index called DBI by the aid of genetic algorithm.

Chapter 4 discusses the methodology into two parts: per pixel spectral-based classifier for detection of hotspots and subpixel spectral-based classifier for hotspot area estimation. Followed by Chapter 5, discusses about the result obtained after performing certain numbers of classification techniques over different satellite data's and the result on the task: subpixel classification for hotspot area estimation. Finally, Chapter 6 provides the concluding remarks and future-scope.

- Its focus is to exploit the tolerance for approximation, uncertainty, imprecision, and partial truth in order to achieve a similar computational behavior as that of human like decision making.

1.1.2 Soft computing preference for satellite images

1. Soft computing is better in handling uncertainty in the data. Thus, it can be used to remove the uncertainties found in satellite images which are introduced due to the dependence of images on the atmospheric conditions. The presence of such uncertainties results in increase in difficulty to create a generic classification model which can classify the same region in different observational conditions.
2. Soft technique approaches can be used to reduce the dimensionality of the input features resulting in simplification of the analysis with reduction in dependability among the features.

1.2 Objective

- Task I:
  a. Critical study of supervised and unsupervised classification techniques by using different satellite data: MODIS, Landsat-5TM and NOAA/AVHRR to detect hotspots.
     - **Supervised classifiers:**
       - Minimum distance
       - Parallelepiped
       - Maximum likelihood
     - **Unsupervised classifiers:**
       - K-means
       - ISODATA
  b. Explore the possibility of soft computing techniques for hotspot detection with higher detection accuracy (HDA) and low false alarm rate (FAR).

CHAPTER 2

BRIEF LITERATURE REVIEW

In this chapter, a brief literature review is performed in correspondence to the application of soft computing techniques over satellite images majorly focusing over detection of coal fires as well as over the various subpixel classification techniques.

2.1 Satellite image analysis for hotspot detection

Satellite images are used for applications such as: change detection, agricultural monitoring, forest fire monitoring, landslide monitoring, natural calamity monitoring etc. Soft computing techniques are majorly used in processing satellite images for various purposes. One among them is the use of Genetic Algorithm (GA) in performing Image fusion [2-3] of satellite images where the weights over the parameter of different images are optimized to give the finest resultant image. Such fusion of satellite data of MODIS and PALSAR using GA was performed by T. Ahmed et al [4] as well as Particle Swarm Optimization (PSO) [5] (instead of GA) to classify hotspot and non-hotspot regions in Jharia, Jharkhand. Also, in this [6], thermal and visual images are fused and a technique which comprises of discrete wavelet transform (DWT) for feature extraction and GA to get better optimized combined image are used while PSO can also be used as the optimizing tool to detect hotspots over the fused image of SAR and MODIS reported by Bushra et al. [7]. Thus, this highlights about the advantage of PSO and GA and it also indicates that the fusion of different satellite data's [8] can be used for our purpose.

Also, determination of hotspots at Jharia using NOAA/AVHRR channel 4, channel 5 and different indices were developed by fuzzy based methodology [9]. The detection accuracy achieved by this algorithm was consistently higher than 80% and maximum detection accuracy achieved was 96%. The use of fuzzy logic have resulted in better performance over the entropy based threshold, multi-threshold and contextual methods.

Since SVM is quite popular, robust technique for image classification [10-12]. Thus, the application of SVM has been analyzed for hotspot detection over Jharia coalfield as well as image analysis techniques were carried on NOAA/AVHRR satellite images [13-14]. Since the

image is of low resolution results in the need of efficient optimization techniques along with the image analysis techniques. The multi-threshold technique is used to remove cloud coverage from land coverage and classify hotspots. While SVM has the advantage over multi-thresholding technique that it can learn patterns from the examples and therefore is used to optimize the performance by removing the false points which are highlighted in the threshold technique. RBF kernel is used to train SVM because it non-linearly maps the samples into a higher dimensional space, so it, unlike the linear kernel, can handle the case when the relation between class labels and attributes is non-linear. Thus, hotspots and non-hotspots can be classified. The performance of the SVM is also compared with the performance obtained from the neural networks and SVM appears to detect hotspots more accurately (greater than 91% classification accuracy) with lesser false alarm rate.

An unsupervised classification technique using genetic algorithm with Davies–Bouldin index (DBI); DBI as fitness function were studied by Bandyopadhyay et al [15] and as unsupervised classification in [16]. It performs clustering by using the centre of cluster which is suggested by GA, as genetic algorithm outputs the optimal cluster centre. The optimal cluster centre is obtained by minimizing the ratio of the sum of within-cluster scatter to between-cluster separation (called DBI). This technique is demonstrated over satellite images as well as real-life datasets [17]. In [18], author proposes a new cluster validation index along with comparisons of various indices such as: DB Index, Dunn's Index, Generalized Dunn's Index. In [19], superiority of GA based K-means over the widely known K-means approach has been studied by analyzing their performance over classifying a satellite image.

Enrico et al [20] proposes the application of NIR region of SAR data for the identification of burned area as the NIR region has the most valuable information about the aspect of burned surface since the decrease of the reflectance value of NIR is observed over such burned surface due to the presence of ash and carbon over the soil. Also, in [21], detection of burn scars using optical dataset (MODIS) is elaborated.

Discussion about the use of thermal data during day and night time, detection of coal fires using multi spectral thermal images were done by Zhang et al. [22] which can be viewed as application of remote sensing for the detection of coal fires. The considered, satellite images are LANDSAT TM, NOAA/AVHRR, ASTER etc.

Also, Walker et al [23] assess the ability of ALOS/PALSAR data over LANDSAT for the estimation of large areas of Land cover and mapping of forest in Brazilian Amazon. It indicates that PALSAR has higher accuracy over the estimation of Land cover when compared with Landsat. The data fusion method was applied over the detection of hotspot by fusing SAR image and optical resolution: MODIS image [24]. Thus, such fusion was found to indicate an efficient method to detect Hotspots with a good accuracy over HDA and FAR.

2.2 Subpixel Analysis

In coarse resolution images such as NOAA/AVHRR, MODIS etc., target to be detected might belong partially within a pixel or are shared among more than one pixel. Thus, such mixed pixels are major problems with the low spatial resolution images, requiring for a better classification rather than hard classification such as Maximum likelihood which are more profound over hard classification, where the pixel will be classified to a class that has highest proportion of spectra value in comparison to other classes. Thus, this leads to inappropriate classification considering smaller target (in comparison to the spatial resolution of satellite image). This drawback can be overcome by performing soft classification which involves classifying a pixel into more than one class in such mixed pixel images. The Linear Mixture Modeling (LMM) is widely known method for sub-pixel classification which is based on the assumption that the spectral response of each pixels is the linear combination of various target classes present within the pixels and each targets are weighted by an abundance fraction such that these fractions are their corresponding proportions of their presence (various target classes) over the ground.

Spectral unmixing approach involves majorly two steps: First, find a pure pixel which consists of only a single ground component of specific target usually known as endmember and second is about estimating the fraction of such endmember present within the mixed pixel spectrum. In [25], author have provided a comparative analysis of various available algorithm for linear spectral unmixing of hyperspectral image. In this study, noise, mixture complexity, use of radiance/reflectance data are investigated for the simulated and real hyperspectral data collected by the Airborne Visible and infrared Imaging Spectrometer (AVIRIS).

Linear spectral unmixing are efficient and effective when target signatures are distinct. In [26], the author have performed linear spectral mixture analysis by imposing constraints on

target signatures rather than target abundance fractions and therefore such techniques are referred as target signature constrained mixed pixel classifiers. Whereas, in [27] authors have proposed a methodology to perform extraction of pure pixel spectral signature from the image data for the purpose of performing linear mixture model. The author have estimated the proportions of target class present within the low spatial resolution of MODIS data using the auxiliary data obtained from the medium spatial resolution (Landsat Enhanced Thematic Mapper Plus) data. The main disadvantage of such linear spectral mixture analysis based approach is that it can be utilized for target detection but under performs for detecting similar targets.

An approach called constrained energy minimization (CEM), which is more effective due to implementation at real time processing; has been proposed to estimate endmembers and detection of targets in multi-spectral and hyperspectral images in [27-31]. The very gain of CEM is its ability to detect small targets effectively. CEM is a constrained target detection method; which is conditioned by constraining over its desired target spectral signature unlike other techniques such as: FCLS (Fully constrained least squares), SCLS (Sum-to-one constrained least squares) and NCLS (Non-negatively constrained least squares) which are constrained on targets abundance fractions [32]. Unlike these techniques, CEM requires only a prior knowledge of target signature while considers other classes as interferers.

An extended version of CEM approach for performing band selection called constrained band selection (CBS) for hyperspectral imagery is proposed in [33]. The proposed technique interprets a band image as a desired target signature while others are neglected as unknown signatures. It is experimented and conveyed that CEM is a robust band-selection technique. Further, in [28], a detection of targets using multispectral imagery is done at subpixel level by generalized constrained energy minimization (GCEM) approach which comprises of dimensionality expansion (DE) approach, to generate additional band which are non-linear combination of original multispectral bands. Thus, such dimensionality expansion aids in the application of CEM over multispectral imagery dataset.

The overall literature review indicates that there are limited works available over the spatial estimation of hotspot coverage using freely available coarse spatial resolution satellite images (esp. MODIS). Hotspot monitoring requires a high temporal resolution dataset for having regular monitoring. Sensors such as MODIS with high temporal resolution (one image per day)

proves to be a better way for monitoring the changes in the hotspot affected areas. But the coarse spatial resolution of MODIS data makes hotspot monitoring a cumbersome task. In order to overcome such drawback, subpixel analysis which has been used in many literatures for different problems can be employed for hotspot detection in subpixel level. Subpixel analysis methods like CEM, could be a better method in detecting small targets efficiently [29-32, 34]. This can be further extended to estimate fractional hotspot area coverage over a region.

CHAPTER 3

THEORETICAL BACKGROUND

In this chapter, a conceptual understanding of various methods or techniques used for performing the tasks such as: Per pixel spectral based classifier for the detection of hotspot by the use of various optical satellite images have been elaborated. Also, the concepts in relate to subpixel classification for area estimation such as: Pixel purity index (PPI), subpixel target detection method etc., have been elaborated.

3.1 Study Area

Jharia coalfield is chosen as the study region. Jharia is situated nearer to Dhanbad town located at 260 km in the North-West of Kolkata and at 1150 km in South-East of Delhi. It is geographical lat/lon are: latitude 23° 35' N to 23° 55' N and longitude 86° 05' E to 86° 30' E as shown in figure: 3.1 and 3.2. The Coal field almost spread around 450 km^2.

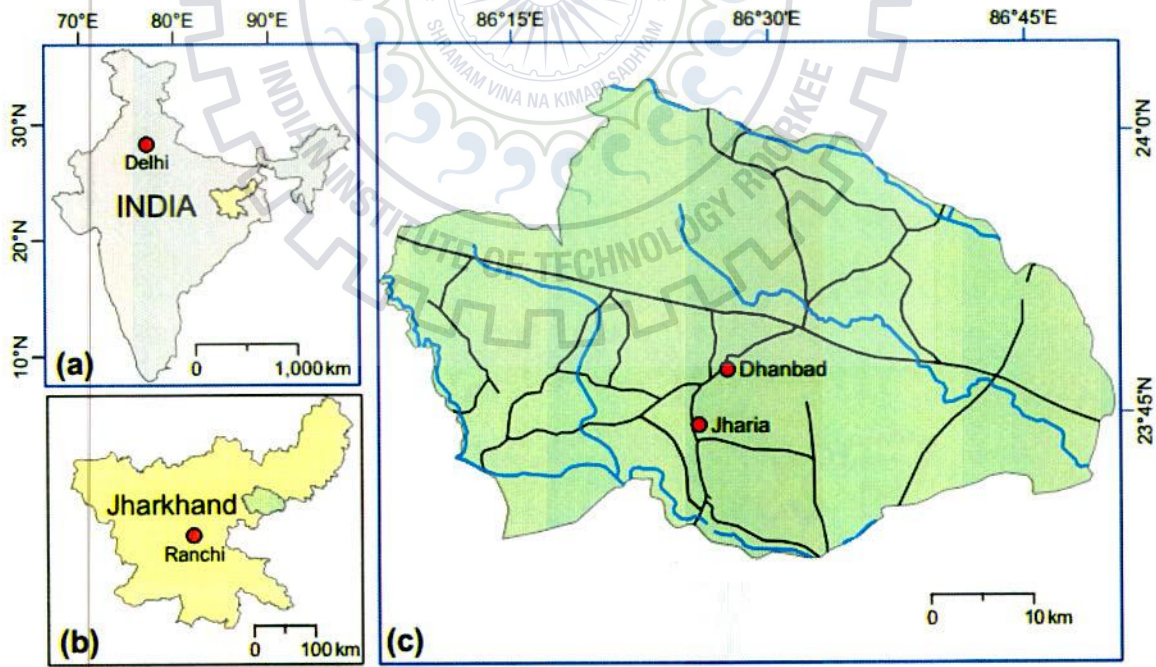

Figure 3.1 Location Map of Jharia, Jharkhand [35]

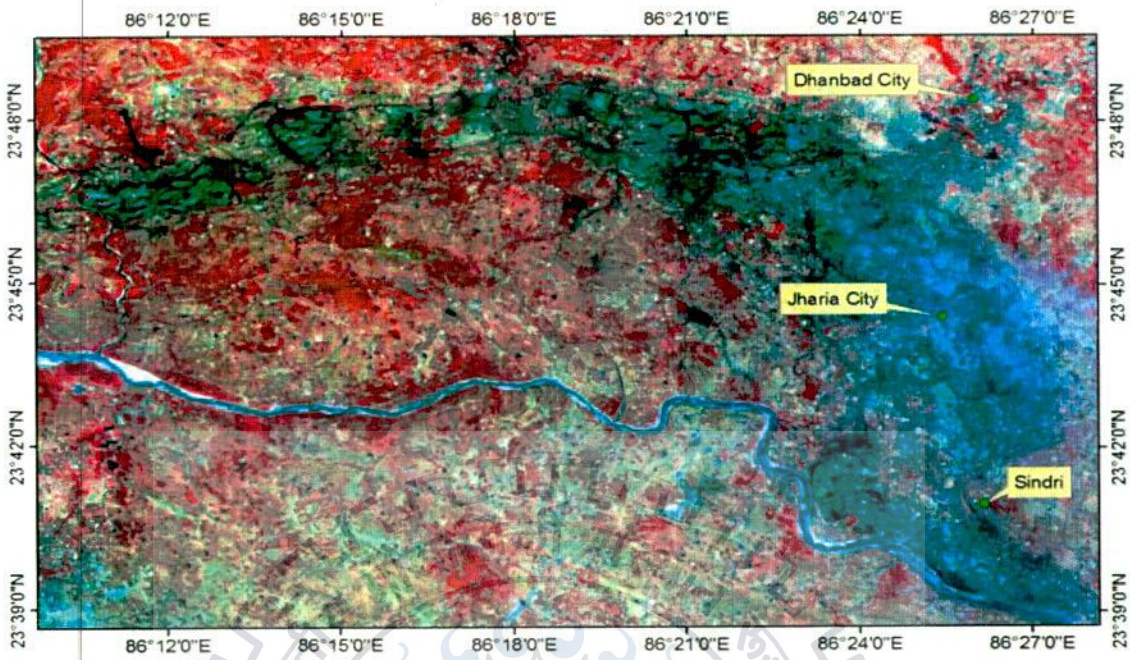

Figure 3.2 Satellite imagery (Landsat-5) of the Jharia coalfield [35]

Attributes of Study Area [1]:

- A major river "Damodar river" is found to flow through our study region.
- This coal field has above 100 coal mines
- In this coal field, there are underground and open-cast mining activities, but majorly open-cast coal fields are noticed.
- The major number of underground mining areas is found to be densely populated about 1.1 million, which are facing adverse effects due to coal fire.

Important subsurface coal fire (hotspots) regions latitude and longitude are mentioned in table 3.1.

Table 3.1 Latitude and longitude of important hotspots in Jharia coalfield [59].

S.No	Latitude	Longitude
1	23°41′22″	86°22′34″
2	23°47′31″	86°18′48″
3	23°48′20″	86°08′37″
4	23°47′34″	86°20′38″
5	23°42′19″	86°25′38″
6	23°44′03″	86°22′02″
7	23°42′25″	86°25′41″
8	23°47′24″	86°11′59″
9	23°44′31″	86°24′23″
10	23°00′14″	86°26′28″

S.No	Latitude	Longitude
11	23°41′17″	86°23′25″
12	23°42′08″	86°25′36″
13	23°45′01″	86°07′24″
14	23°39′32″	86°27′02″
15	23°47′24″	86°17′30″
16	23°46′28″	86°09′51″
17	23°47′58″	86°27′02″
18	23°47′53″	86°13′06″
19	23°48′19″	86°22′41″
20	23°46′44″	86°19′30″

S.No	Latitude	Longitude
21	23°45′13″	86°24′00″
22	23°47′04″	86°18′57″
23	23°47′02″	86°16′31″
24	23°43′58″	86°26′39″
25	23°46′09″	86°21′41″
26	23°42′38″	86°25′18″
27	23°42′33″	86°27′06″
28	23°42′53″	86°23′23″
29	23°44′11″	86°25′14″
30	23°47′50″	86°15′49″

3.2 Satellite images used

The satellite Images can be broadly classified into two categories (as shown in fig. 3.3) based on the sensor used. These two types are:

1. Passive sensors
2. Active sensors

Passive sensors use the natural energy to identify the object. These natural energies are emitted or reflected by the target or target surrounding. Infra-red, charge-coupled devices, radiometers can be called as examples of passive sensors. While on the other hand, the active sensors are those which doesn't depend on natural energy instead it uses its own energy as the source and this is reflected or backscattered by the target. The speed and round trip delay (between emission and return) of the source energy is used to find the characteristics of the target.

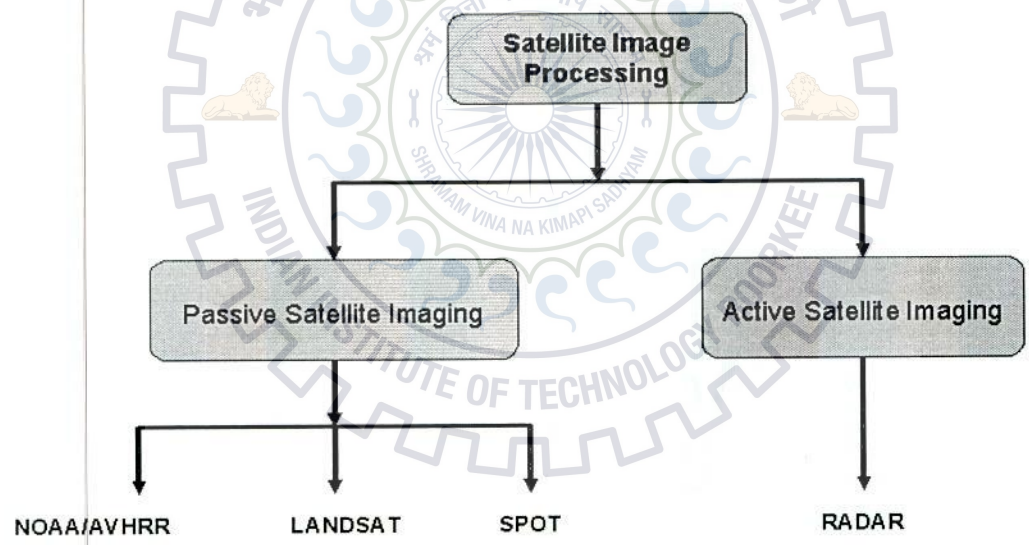

Figure 3.3 Types of satellite imaging with examples [34]

In addition to availability of satellite images in different resolution; the satellite images can be distinguished based on the spectral channels of variable wavelength. Each of these channels has its own significance and they are unique to the respective applications. For example,

a. Thermal channels are useful to monitor temperature variation aspects such as forest fire, ocean current variations
b. Visible and near-infrared are very suitable to monitor cloud, water and agriculture.

Additively, other indices such as NDVI, MSAVI are used to measure the vegetation index and soil characteristics respectively.

The statistical methods applied on these channels such as: fusion of different bands etc. can be an added advantage as they improve the features of utilizing the satellite images as such fusion of different bands has been used as an approach to detect hotspots.

Satellite data comprises of an image where each pixel of this image called DN value indicates the spectral signature of an object within the pixel. The satellite images can be varied based on spatial, temporal and spectral resolution.

3.2.1 Moderate-resolution imaging spectroradiometer (MODIS) Data

MODIS is the payload launched by NASA by boarding it to TERRA satellite in 1999 and boarded AQUA satellite by 2002. This instrument contains 36 bands ranging in wavelength from 0.4 μm to 14.4 μm and at varying spatial resolutions (2 bands at 250 m, 5 bands at 500 m and 29 bands at 1 km). Thus, It could create the entire earth image in every 1 or 2 days. The main objective of MODIS is to provide earth dynamics such as: change in cloud cover, radiation budget, and wildfire. MODIS spatial Resolution is: 250 m (bands 1–2) 500 m (bands 3–7) 1000 m (bands 8–36). The MODIS bands and its uses are shown in table 3.2.

Table 3.2 MODIS bands

Band	Wavelength (nm)	Resolution (m)	Primary Use
1	620–670	250	Land/Cloud/Aerosols Boundaries
2	841–876	250	
3	459–479	500	Land/Cloud/Aerosols Properties
4	545–565	500	
5	1230–1250	500	
6	1628–1652	500	

7	2105–2155	500	
8	405–420	1000	Ocean Color/ Phytoplankton/ Biogeochemistry
9	438–448	1000	
10	483–493	1000	
11	526–536	1000	
12	546–556	1000	
13	662–672	1000	
14	673–683	1000	
15	743–753	1000	
16	862–877	1000	
17	890–920	1000	Atmospheric Water Vapor
18	931–941	1000	
19	915–965	1000	
20	3.660–3.840	1000	Surface/Cloud Temperature
21	3.929–3.989	1000	
22	3.929–3.989	1000	
23	4.020–4.080	1000	
24	4.433–4.498	1000	Atmospheric Temperature
25	4.482–4.549	1000	
26	1.360–1.390	1000	Cirrus Clouds Water Vapor
27	6.535–6.895	1000	
28	7.175–7.475	1000	
29	8.400–8.700	1000	Cloud Properties
30	9.580–9.880	1000	Ozone
31	10.780–11.280	1000	Surface/Cloud Temperature
32	11.770–12.270	1000	
33	13.185–13.485	1000	Cloud Top Altitude
34	13.485–13.785	1000	
35	13.785–14.085	1000	
36	14.085–14.385	1000	

3.2.2 Advanced very high resolution radiometer (AVHRR) Data

AVHRR is a space-borne sensor which measures the earth reflectance in 5 wide spectral bands. It has been carried by NOAA family of polar orbiting platforms. NOAA has at least two polar-orbiting meteorological satellites in orbit at all times where one satellite crosses the equator in early morning and early evening and the other crossing the equator in the afternoon and late evening with respect to (Indian Standard Time) IST. Together they provide twice-daily global coverage such that data for any region of the earth are no more than six hours old. The main purpose of AVHRR is to study climate change, monitor clouds and to measure thermal emission of earth.

NOAA/AVHRR image comprises five spectral bands: visible (ch.1, 0.63 μm), near-infrared (ch.2, 0.83 μm), mid-infrared (ch.3, 3.75 μm), and thermal (ch.4-5, 10-12 μm). The highest ground resolution that can be achieved by NOAA/AVHRR is 1.1 kilometer; it means the minimal amount of area that can be shown in a pixel is 1.1 x 1.1 km^2 area. The channels and its corresponding usages are shown in table: 3.3.

Table 3.3 AVHRR Spectral Characteristics

Channel No.	Wavelength	Typical use
1	0.58 – 0.68	Daytime cloud, haze and surface mapping
2	0.725 – 1.00	Land-water boundaries
3	3.55 – 3.93	Night cloud mapping, sea surface temperature
3A	N/A	Snow and ice detection
3B	N/A	Night cloud mapping, sea surface temperature
4	10.30 – 11.30	Night cloud mapping, sea surface temperature
5	11.50 – 12.50	Sea surface temperature

3.2.3 LANDSAT Data

Landsat is the world's longest continuously acquired collection of satellite based moderate-resolution land remote sensing data. It provides a unique resource for those who work in agriculture, forestry, regional planning, geology, and global change research etc., Landsat images are also invaluable for emergency response and disaster relief. For over 40 years, the Landsat program has collected spectral information from Earth's surface, creating a historical archive unmatched in quality, detail, coverage, and length. It has moderate-spatial resolution.

The latest series- Landsat-8 has the following 11 bands as shown in table 3.4.

Table 3.4 LANDSAT-8 bands

Band Number	µm	Resolution
1	0.433–0.453	30 m
2	0.450–0.515	30 m
3	0.525–0.600	30 m
4	0.630–0.680	30 m
5	0.845–0.885	30 m
6	1.560–1.660	30 m
7	2.100–2.300	30 m
8	0.500–0.680	15 m
9	1.360–1.390	30 m
10	10.6-11.2	100 m
11	11.5-12.5	100 m

Bands 1-4 and 8 senses visible light; Band 5 measures near-infrared; Bands 6 and 7 cover different slices of the shortwave infrared; Band 9 covers a very thin slice of wavelengths: only 1370 ± 10 nanometers. Thus, Band 9 is meant to capture very bright/clearly visible object. Bands 10 and 11 are in the thermal infrared.

For our study, we have considered Landsat 5 Thematic Mapper (TM). Landsat-5TM images consist of seven spectral bands with a spatial resolution of 30 meters for bands 1-5 and 7 while band-6 is 120 meters which is resample to 30-meter pixels. The various bands and its corresponding usages are mentioned in table 3.5.

Table 3.5 Spectral Characteristics of LANDSAT -5 TM

Band	Wavelength	Useful for mapping
Band 1 - blue	0.45 - 0.52	Bathymetric mapping, distinguishing soil from vegetation and deciduous from coniferous vegetation
Band 2 - green	0.52 - 0.60	Emphasizes peak vegetation, which is useful for assessing plant vigor
Band 3 - red	0.63 - 0.69	Discriminates vegetation slopes
Band 4 - Near Infrared	0.77 - 0.90	Emphasizes biomass content and shorelines
Band 5 - Short-wave Infrared	1.55 - 1.75	Discriminates moisture content of soil and vegetation; penetrates thin clouds
Band 6 - Thermal Infrared	10.40 - 12.50	Thermal mapping and estimated soil moisture
Band 7 - Short-wave Infrared	2.09 - 2.35	Hydrothermally altered rocks associated with mineral deposits

3.3 Preprocessing of different optical satellite data

Optical images that are available from sensors like MODIS, NOAA/AVHRR, Landsat are available as pre-processed data. These data are available in sinusoidal projection and are thus converted to Geographic Lat/Lon projection (WGS-84).

3.4 Useful information to be extracted from satellite data

The Normalized Difference Vegetation Index (NDVI) is one of the most commonly used index for measuring the greenness and vegetation abundance over a region. It aid to distinguish between Green vegetation and soil brightness. It is a ratio image formed by the composite of NIR and RED bands which is mathematically expressed as

$$NDVI = \frac{\Phi_{NIR} - \Phi_{RED}}{\Phi_{NIR} + \Phi_{RED}} \quad (1)$$

The NDVI value falls within the range of -1 to +1. Positive NDVI refers to presence of vegetation whereas negative refers to presence of water bodies or no vegetation. NDVI value falling around zero is a physical significance of presence of bare soil ground or rock.

NDVI plays an important role for the detection of hotspot due to the fact that hotspot region usually has bare ground such that neither bushes nor grasses grows over hotspot region.

Thus, vegetation's are not observed over the hotspot region as such hot subsurface doesn't yield vegetation [36-39]. Generally, vegetation has a low correlation between the visible and NIR bands due to the strong absorption of NIR bands but high reflectance of red band [36]. Thus, unfit lands to support vegetation over the subsurface areas could be identified by the use of RED and NIR bands.

Table 3.6 Optical satellite data used for the study

S.no	Data	Acquisition ID	Acquisition Date	NDVI		Data ID
				NIR Band	Red Band	
1	LANDSAT-5TM	LT514004320110 86BKT01	26-Mar-2011	Band 4	Band 3	LST1
2		LT514004420110 86BKT01	27-Mar-2011			LST2
3	MODIS	MOD09Q1.A2011113.h25v06.005.2011123032639	23-Apr-2011	Band 2	Band 1	MOD 1
4		MOD09Q1.A2012081.h25v06.005.2012096143505	21-Mar-2012			MOD 2
5		MOD09Q1.A2015073.h25v06.005.2015083112326	14-Mar-2015			MOD 3
6		MOD09Q1.A2015089.h25v06.005.2015098081632	30-Mar-2015			MOD 4
7	NOAA/AVHRR	NSS.LHRR.NP.D11111.S0720.E0732.B1133636.WI	21-Apr-2011	Band 2	Band 1	AVH 1

The table 3.6 indicates various datasets used for performing our tasks. MOD1, AVH1 and LST1 are used for performing per-pixel spectral based classification. And LST2, MOD2, MOD3 and MOD4 were used for performing subpixel spectral based classification for performing hotspot area coverage over Jharia region.

3.5 Per pixel spectral-based classification

Satellite images are classified to various target classes based on the effective presence of a specific target class in comparison to other target classes within the image. The satellite images can be classified based on spectral and spatial properties but majority of image classifications are based merely on spectral signatures of target classes. In such spectral based classifiers, classification is performed based on the statistical parameters of each pixel spectral values and they are assigned to a single class but cannot be assigned to more than one class. But usually, due to the difference of spatial measurement between the satellite image and its corresponding ground measurement are varied; thus a pixel would comprise many target classes and these pixels are called mixed pixels. In order to classify such mixed pixels, the statistical characteristic of each class is calculated and this pixel is classified into a target class of higher proportion in comparison to other class proportions. Thus, such classification based on spectral attributes of the image is called per pixel spectral based classifier.

In our problem, the overall objective is to classify pixels into their respective feature classes: hotspot and non-hotspot, which are performed according to the classification algorithm. Image classification is performed by classifying the NDVI image of the corresponding satellite dataset by applying learning algorithms to classify all pixels in an image to fall into the feature classes based on predefined classification model. The classifiers used to perform image classification can be broadly divided into categories such as: supervised classifiers, unsupervised classifiers. The classified image are then assessed by metrics- HDA and FAR as discussed in section 3.7.

3.5.1 Supervised classification

It involves performing classification by training the classifier using the user input training samples collected as ground truth point with the information of them belonging to respective feature classes. These collected training samples are feed to the classification algorithm along with the input image (to be classified) resulting in pixels classified to the respective feature classes.

Generally, there are three major steps involved in supervised classification:

Step 1: Training

Collection of some training points from the representative training area are performed under training phase as these training data points are the numerical description of the spectral attributes of each feature class.

Step 2: Classification

Each pixel in the image is classified into a class which has higher resemblance over the other. The weighting of each class is measured using the training points. If a pixel doesn't resemble any of the feature classes, will be labeled as unknown.

Step 3: Accuracy assessment

The Classified image is compared with some reference image or ground truth points in order to calculate the accuracy of classification.

Hotspot and non-hotspot are the two target classes to which all the pixels are classified into. The collected ground truth point are used as the training point for the classifiers and each classifier will give a resultant classified image.

There are various types of supervised classification techniques. Some of the techniques which have been used in our problem is briefed in the below subsection.

3.5.1.1 Types of supervised classification

I. Maximum likelihood classification:

This involves classifying the input image into corresponding feature classes by evaluating variance and co-variance of the categorical spectral response pattern of the image. It works with an assumption of the data being classified has a Gaussian distribution. Thus, the statistical parameters such as: mean and co-variance of the training data are utilized to classify an unknown pixel into the respective feature class by calculating its conditional probability of belonging to a particular class [40]. The multivariate normal distribution is used to describe that a pixel x belonging to a class k as:

$$\phi_k(X_i) = (2\pi)^{-1/2p} |\Sigma_k|^{-1/2} \times e^{-1/2(X-\mu_k)\Sigma_k^{-1}(X-\mu_k)} \qquad (2)$$


भारतीय प्रौद्योगिकी संस्थान रुड़की
श्रमं विना न किमपि साध्यम
SHRAMAM VINA NA KIMAPI SADHYAM
INDIAN INSTITUTE OF TECHNOLOGY ROORKEE

II. Minimum distance classifier:

The minimum distance classifier can also be called as a mean - distance classifier as it involves assigning an unknown pixel to a respective class based on its minimal distance between the pixel to be classified and the mean of classes [40]. The distance between the pixel and the class mean are called as the similarity index, lesser the distance between them means higher its similarity index. The concept of minimum distance classifier is shown in figure 3.4.

The following distance measures are often considered:

1. Euclidean distance:

The Euclidean distance is calculated by

$$d_k^{\,2} = (X - \mu_k)^t \cdot (X - \mu_k) \qquad (3)$$

Where

X: Vector of Image data (n bands)

$X = [x_1, x_2 ....., x_n]$

$\mu_k = [m_1, m_2, ..., m_n]$

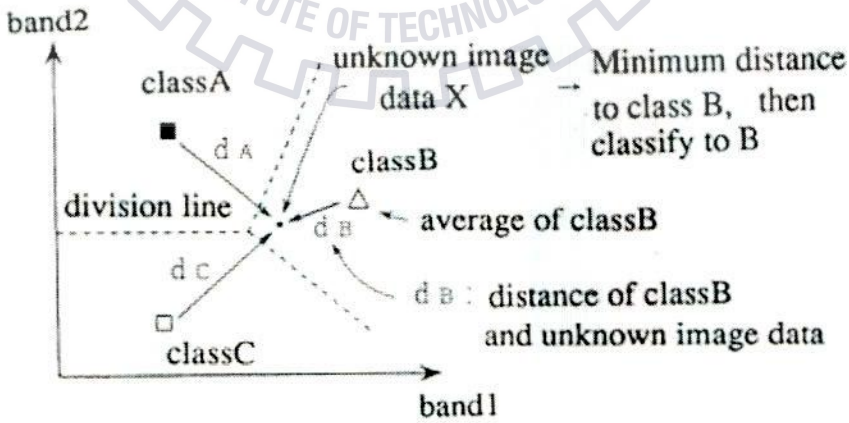

Figure 3.4 Concept of Minimum Distance Classifier [41]

The minimum distance classifier is considered to be computationally faster, but it is not as flexible as a maximum likelihood classifier as it doesn't use covariance data.

III. Parallelepiped classifier:

The Parallelepiped classifiers are normally referred as box classifier. It is a Rule-based algorithm where the threshold of each class signature is used to decide to which class a pixel belongs. The class signature is derived from the statistical calculation of analyst defined training samples [40]. A pixel is classified as a member of a class when this pixel value falls between the ranges of a class signature whereas whenever there is a overlapping among more than one class then it assigned to the first class while unclassified pixels are to a class called unknown class.

3.5.2 Unsupervised classification

It is the classification to classify pixels into a group of pixels having similar characteristics without using any training data. But it requires user's knowledge of the area being classified as he must be aware to relate it to the actual feature over the ground. In our problem, the image to be classified is NDVI image and it is classified into two target classes: hotspot and non-hotspot.

3.5.2.1 Types of unsupervised classification

I. K-means

K-means is one of the simplest algorithm known to classify (group similar pixels) in a less computational time. K-means tries to group similar pixels based on measuring the distance between the centre of clusters and the pixel. The pixel is assigned to a cluster which has high similarity index (closer to the center) [40]. K-means requires explicit indication of number of clusters.

Below are the brief steps followed in K-means:

Step 1: Choose initial cluster centre randomly

Step 2: Assign pixels to the clusters which has high similarity index.

Step 3: Compute new centre for the clusters.

Step 4: Iterate the above steps from step 2 and 3 until movement of cluster centers are below the threshold.

II. ISODATA

ISODATA works in similar to K-means with the distinct difference that it doesn't require a prior knowledge about "Number of clusters" [40]. Thus, it can be seen as a specific refinement over K-Means algorithm. These specific refinements are:

i. Clusters with few members are discarded.
ii. Too many member clusters are split into two new clusters.
iii. Clusters that are too spread are split into two groups.
iv. Clusters are merged if their centers are too close.

Below are the brief steps followed in ISODATA:

Step 1: Cluster centers are randomly chosen while non-centre members are assigned to a cluster based on its shortest distance to the center.

Step 2: Distance between center of clusters as well as standard deviation within the cluster are calculated such that:

- Clusters are split if standard deviations are more than the user-defined threshold.
- Clusters are merged if the distance between cluster centre's are less than the user-specified threshold.

Step 3: Repeat the above steps with new cluster centre's.

Step 4: Iterations are performed until:

- Average inter-cluster centre distance is below the user-defined threshold.
- Average change between the inter-cluster centre among iterations are below the threshold or the maximum number of iteration is met.


भारतीय प्रौद्योगिकी संस्थान रुड़की
श्रमं विना न किमपि साध्यम्
SHRAMAM VINA NA KIMAPI SADHYAM
INDIAN INSTITUTE OF TECHNOLOGY ROORKEE

3.5.3 Classification with commonly used soft computing technique

Soft computing aims to exploit the tolerance for imprecision, uncertainty, approximate reasoning and partial truth in order to achieve tractability, robustness and low-cost solutions. Genetic algorithm is a widely known soft computing technique which mimics the process of natural selection process.

3.5.3.1 Genetic algorithm

Genetic algorithms follows the adaptive heuristic search algorithm which involves competition among individuals for scanty resources resulting in fittest individuals dominates over the weaker ones. In brief, GA follows the Darwin theory- survival of the fittest [43]. Thus, it is an idea of natural selection. Though they seem randomized but GAs is by no means random, instead they exploit the probabilistic nature of the problem to direct the search into the region of better performance within the search space. In short, they try to simulate processes in natural systems necessary for evolution.

GAs terminology is analogous to that used by biologists. As shown in the table: 3.7:

Table 3.7 GA terminology [43]

Biological	GA
Chromosome or genotype	Structure, or string (often binary)
Locus	A particular (bit) position on the string
Phenotype	Parameter set or solution vector (real-valued)

GAs contains a population of individuals (pool of hypothesis) to guess initially within the search space. These populations are usually selected random out of the entire search space. These individuals are mostly encoded as binary values (i.e., base-2) but in recent years, use of real values (base-10) is highly noticed [43]. These encoded individuals are used by further GA operators such as: selection, crossover, mutation in the following order.

Step 1: Selection

It is used to select the best individual out of the entire population which will be considered in further generation as similar to natural selection found in biological systems [44]. Poorer performing individuals are neglected while those individuals better than the average will be considered as the finest individual to be considered further operations. These evaluation is based

on an objective function (i.e. fitness function) [43]. The pictorial explanation of selection operator is shown in fig. 3.5.

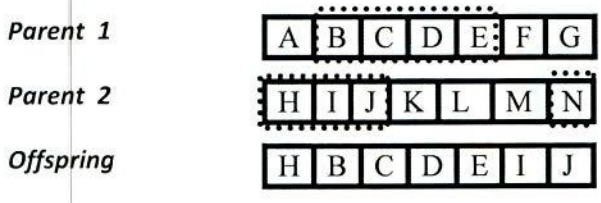

Figure 3.5 Selection Operator

Step 2: Crossover Operator

The individuals selected by selection operator are considered for crossover. Crossover allows exchange of information among the parent individuals as similar to exchange of genes among the chromosomes in natural selection analogy. Based on the number of locus chosen and randomly choosing this locus within in considered individuals, lets the two individuals to swap all the information across the locus point [43].

Crossover can be of two types: single point crossover and double point crossover based on the number of locus considered.

Eg: *Single Point Crossover:*

If **Parent$_1$** = 000000 & **Parent$_2$** = 111111

While the locus is 2 then,

Parent$_1$' = 110000 & **Parent$_2$'** = 001111

This new offspring's are included into the population of next generation.

Step 3: Mutation Operator

Mutation is used to randomly flip one/more bits within an individual. Rate of mutation is always kept minimal compared to crossover as mutation results in a random walk through the search space whereas mutation with selection (without crossover) creates a noise-tolerant, hill-climbing algorithm [18]. In brief, mutation operator is to stimulate diversity within the population.

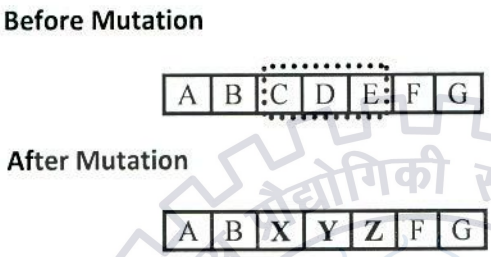

Figure 3.6 Mutation Operator

After performing the above operations, a new population is formed comprising these offspring's after the removal of old parents as the size of the population has to be kept intact. This results in completion of a generation. The pictorial explanation of mutation operator is shown in fig. 3.6.

These processes of selection, crossover and mutation are performed again and again with the new set of individuals until the termination criteria are met. The termination criteria can be: exceeding the time limit of execution time, maximum generations etc.

In brief, GA is used to search a pool of hypothesis in order to find the best hypothesis. The measure of selecting the hypothesis is based on a numerical function called fitness function. The fitness function called K-means index is used to perform hotspot detection which is as described in the following subsection.

GA-KMI *clustering* (KMI as *fitness function*)

GA KMI is performed to classify an image into its feature classes by performing GA operations using K-means index as its fitness function. This fitness value is used as a guide to the stochastic selection of chromosomes which are then considered for further operation: crossover and mutation. Crossover generates new chromosome by performing single point crossover over two

or more selected parents [15, 18]. Mutation acts by randomly selecting genes to be altered thereby avoiding the persistence of local-optimal solutions and thereby improving the diversity within population.

Step 1: String Representation

In GA-KMI, the chromosomes were made up of real numbers and the length of chromosome is equivalent to the number of clusters as each gene on chromosome refers to the centre of cluster [15].

Step 2: Population Initialization

For each string i in the population (i=1, 2… P where is the size of population), i refers to the value of cluster centre. Since, the number of cluster is known a prior, the length of chromosome is fixed as each chromosome comprises of n genes (n refers to number of clusters) and these centre's are chosen randomly from the data set as well as distributed randomly in the chromosomes [15].

Step 3: Fitness Computation

The fitness of a chromosome is computed using K-Means Index. This index is to group similar pixels within in an image based on its distance between the pixel and its centre.

$$\mu_{kn} = \begin{Bmatrix} 1; \|x_n - u_k\| \le \|x_n - u_j\| \\ 0; \quad otherwise \end{Bmatrix} 1 \le k, j \le K; j \ne k; 1 \le n \le N \qquad (4)$$

x_n = pixel n with grey values x (one for each band).

N = Total number of pixels.

μ_{kn} = indicator variable of each pixel belonging to cluster k.

$$v_k = \frac{\sum_{n=1}^{M} (\mu_{kn}) x_n}{\sum_{n=1}^{M} \mu_{kn}} \qquad (5)$$

v_k = average value of each cluster

$$KMI = \frac{1}{(\sum_{i=1}^{k} \|x_i - v_k\|^2)^{1/2}} \quad (6)$$

After termination of the algorithm, an elite chromosome is given which comprises of those cluster centres which have been very closer to its mean value when compared between the distance of cluster centres and their respective means found in other chromosomes. The entire flow of above described steps are shown in fig 3.7.

In our problem, the aim of GA-KMI is to classify the NDVI image into classes: hotspot and non-hotspot. Thus, two clusters are required to be formed such the formed cluster is optimal. This is done by assigning each chromosomes with the pixel values randomly chosen among the entire image such that the elite chromosome suggested after the termination of GA-KMI will contain the optimal cluster centre. Thus, the clusters (clusters: hotspot and non-hotspot) formed is the optimal cluster.

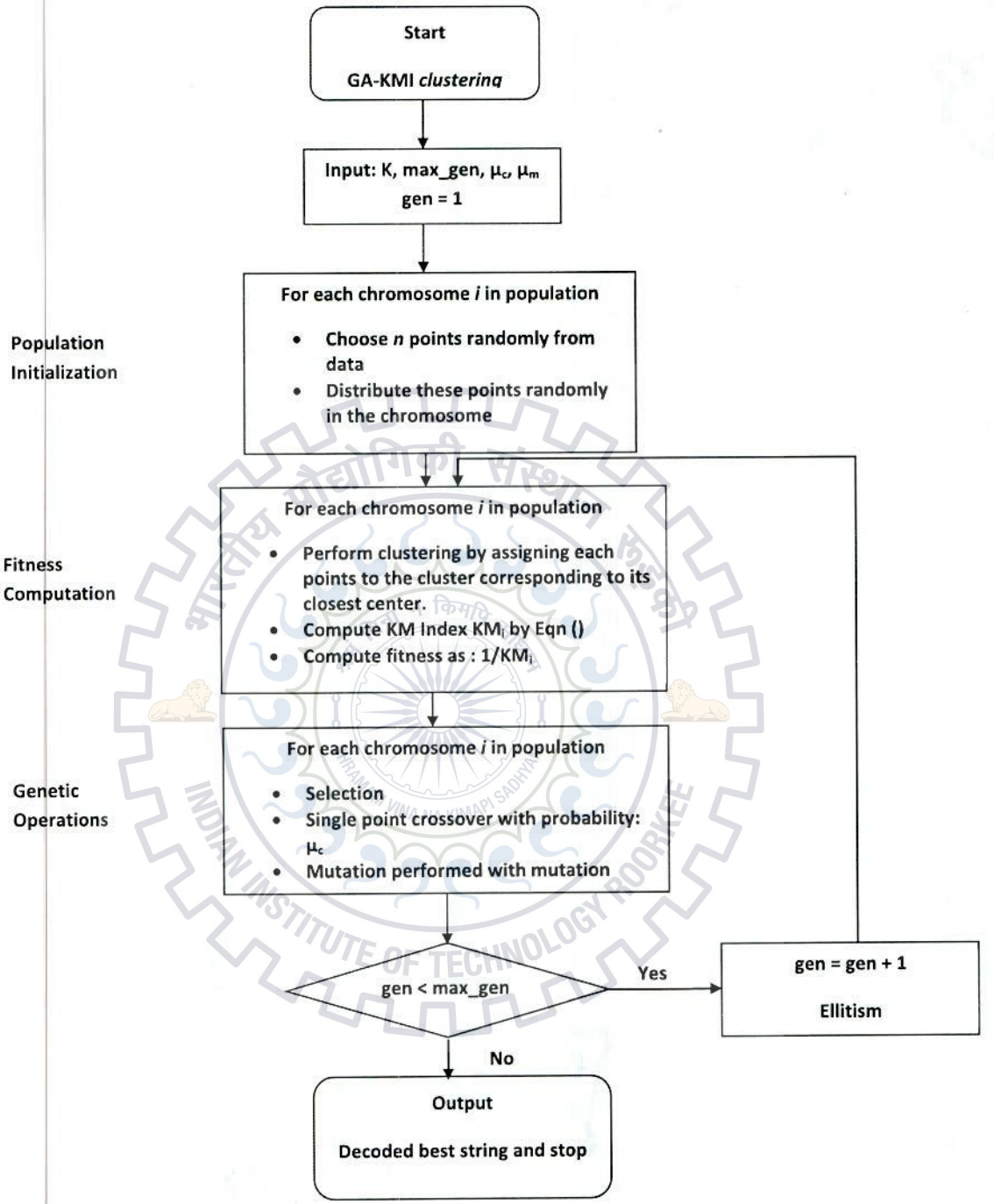

Figure 3.7 Flowchart of GA-KMI clustering

3.6 Assessment of hotspot detection using HDA and FAR

The classified images are assessed using HDA and FAR [14] in order to measure the accuracy of classification algorithms over segregating pixels based on its class feature: hotspot and non-hotspot.

The accuracy of detecting hotspot is calculated as:

$$HDA = \frac{Correctly\ Detected\ Hotspots}{Total\ Hotspots\ That\ Exist} \tag{7}$$

While False Alarm Rate is calculated as:

$$FAR = \frac{Incorrectly\ Detected\ Hotspots}{(Total\ No.\ of\ Pixels - Total\ Hotspots\ That\ Exist)} \tag{8}$$

The classifier should behave in such a way that it gives higher HDA while retaining a low upper bound over FAR.

The entire flow chart of per pixel spectral-based classifier is depicted in fig. 3.8.

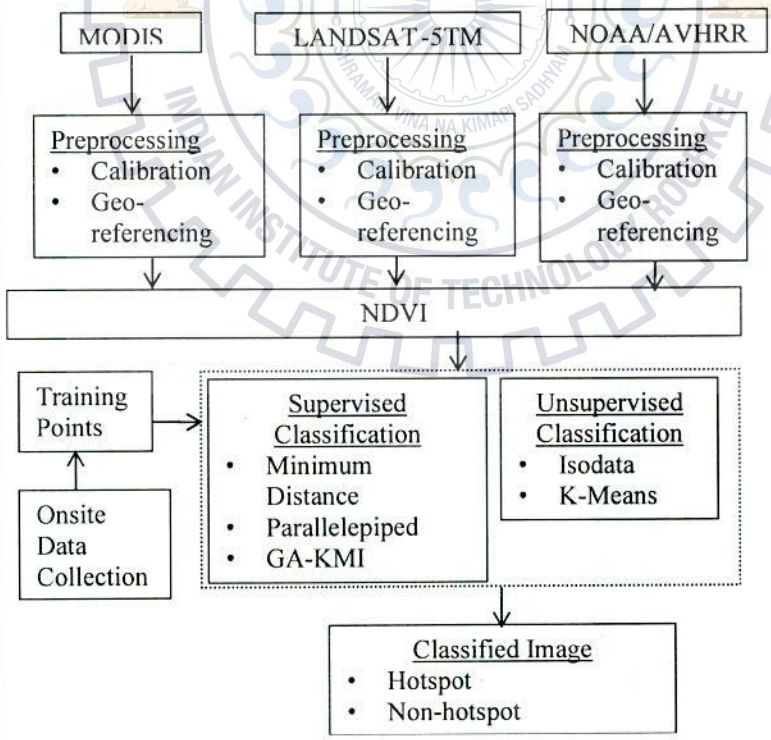

Figure 3.8 Flow chart for detection of hotspots by per-pixel classification

3.7 Area estimation using subpixel spectral-based classification

A pixel of a coarse resolution satellite image (eg: MODIS) might comprise of many classes (eg: urban, vegetation, land, water etc.,) within a pixel, which is due to the fact that the ground sampling distance is much larger than the size of individual class. These pixels are generally called as mixed pixels. This study focuses on area estimation of hotspot coverage over Jharia region at subpixel scale on MODIS dataset.

High hotspot detection accuracy (HDA) and low false alarm rate (FAR) from a classified image is required for better area estimation. While analyzing the dataset, water was giving higher FAR. Therefore, it is important to mask water areas. Land cover classification into three classes: hotspot, non-hotspot and water have been critically analyzed using various classification techniques, and it is found that SVM gives a better classification accuracy. The obtained hotspot classified image will be providing a suspected hotspot prone zone. Therefore, for estimating the area, subpixel analysis is required. Though there are various subpixel method such as: NCLS, FCLS, OSP but CEM is found to be an effective method since it requires only the prior knowledge of hotspot spectral signature and also, unlike other methods, CEM is quite efficient in the detection of smaller targets very effectively. Thus, CEM is being considered for our problem and it is performed over the obtained hotspot classified image.

The detected hotspots from the classified image are then further refined by constrained energy minimization (CEM) for the better estimate of hotspot present on MODIS mixed pixels. These fractions of hotspots computed from CEM method is then segmented into various levels of hotspot density using segmentation technique called GA-DBI. CEM requires a prior knowledge of hotspot spectral signature which is obtained by endmember extraction technique called pure pixel index (PPI). The following entire section of this chapter gives a brief description of each of the above mentioned techniques.

The following steps have been proposed for performing area estimation of hotspot coverage.

Step 1: Image classification

As discussed in section 3.5.1 and 3.5.2, there are various classification techniques available for performing image classification. In order to perform land cover classification (target classes:

hotspot, non-hotspot and water) with an intent to obtain high accuracy; SVM is found to be the appropriate classification technique as it results in higher kappa coefficient and higher overall accuracy in compared to other classification techniques. Support vector machine has been formulated using statistical learning theory [45]. They have been widely popular for being robust like other nonparametric classifiers [46, 47]. SVMs works by nonlinear projecting the training data from input space over to a feature space of higher (infinite) dimension which is achieved by the aid of kernel functions. Such projection results in linearly separable dataset which can be separated by a linear classifier. Thus, such process aides for the classification of satellite images which are of higher dimension input space and cannot be linearly separated. Usually classification in higher dimension space results in over-fitting, however, in SVM over-fitting is constrained by a principle of structured risk minimization [45]. The margin between the decision boundary and the data points are maximized for the minimization of empirical risk of misclassification. In practice, such criteria are met by minimizing a cost factor which involves both the complexity of the classifier and the degree of marginal points that are misclassified. This tradeoff is combined as an error parameter which is selected by performing cross-validation procedures.

The projection from input space to higher space are performed by the aide of kernels such as: Polynomial, Gaussian (aka RBF) etc., a deeper mathematical discussion can be found in [45, 48, 49].

Step 2: Computation of pixel purity index (PPI)

While performing spectral unmixing, the first step is to determine the spectral response of purest pixels or endmembers (of hotspot) in the image. Thus, to find such appropriate image endmembers for spectral mixture analysis, the purest hotspot signature has to be obtained by the aid of PPI. PPI is a widely used endmember extraction technique where endmember is defined as idealized pure signature of a class for example vegetation, urban, water classes. Though there are many other such endmember extraction techniques [50, 51]: N-FINDR, Convex cone analysis, simulated annealing algorithm (SAA) but PPI is widely used due to its easy use and its availability as a module with in the commercial product called ENVI. The PPI technique involves search for a set of vertices of a convex hull in an L-dimensional hyper or multispectral image cube. As a pre-requisite of PPI algorithm, the data sample vectors (pixels) are usually

maximum noise fraction (MNF) transformed such that to reduce dimensionality of the dataset and to perform noise whitening process [52]. Thus, these MNF transformed dataset is projected over a large set of random unit vectors called "skewers" of L-dimension (size of image cube).And, for n-iterations (n is set explicitly) all data sample vectors are projected onto each skewers such that extremity score for the extreme data sample vectors are computed for each iteration and they are cumulatively recorded and such recorded scores are considered as pixel purity index for the respective pixel. Endmember extraction is done by comparing such pixel against target spectra which ever pixel is found to be closer to target spectra is called as endmember.

PPI Algorithm can be briefly written as [53]:

Initialization: Apply maximum noise fraction (MNF) transform to perform reduction of dimensionality of the dataset and k unit vectors called "skewers", $\{\text{skewer}_j\}_{j=1}^{k}$ be generated randomly; k be a large sufficient positive integer.

PPI Calculation: For each skewer$_j$, all data sample vectors are projected onto skewer$_j$ such that to find extreme positioned vectors and form extrema set denoted by $S_{extrema}$ (skewer$_j$) for each skewer$_j$ which comprises of all such extreme positioned vectors. Despite the fact, a different skewer$_j$ generates a different extrema set $S_{extrema}$ (skewer$_j$), it is very likely some sample vectors may appear in more than one extrema set.

As a requirement of pure hotspot spectral signature for performing subpixel analysis, we find such pure spectral signature with the aid of PPI; by applying PPI on a high resolution image (i.e., Landsat-5TM), it results in an endmember which is a pure pixel that comprises of only hotspot as its component.

Step 3: Subpixel hotspot detection using CEM

After obtaining the pure spectral signature and the hotspot classified image, there is a need for identifying target in subpixel level. This can be performed using subpixel target detection method. The detection of specific target using only spatial properties will be cumbersome; thus incorporating spectral property can improve hotspot detection. The spectral properties such as

variability, spectral contrast, similarity can be used to perform target detection at subpixel level [32].

Usually a hyper or multispectral image is represented as an image cube; an image pixel cube is typically represented as an L - dimensional vector where L represents the number of spectral bands.

Linear spectral mixture analysis has been widely used for subpixel detection where the spectral signatures of an image pixel vector $\boldsymbol{r}$ is represented as linear combination of target spectral signatures ($\boldsymbol{m}_1, \boldsymbol{m}_2 \ldots \boldsymbol{m}_p$) with their appropriate abundance fractions specified by $\alpha_1,\alpha_2 \ldots \alpha_p$.

In general, the following constraints:

Abundance sum-to-one constraint (ASC) *formulated* as,

$$ASC = \sum_{j=0}^{p} \alpha^j = 1 \; \mathrm{ASC} = \sum_{j=0}^{p} \alpha^j = 1 \; and \tag{9}$$

Abundance non-negativity constraint (ANC) *formulated* as,

$$ANC = \boldsymbol{\alpha_j} \geq \mathbf{0} \text{ for all } \mathbf{1} \leq \boldsymbol{j} \leq \boldsymbol{p}. \tag{10}$$

In brief [32], various LSMA approaches were formed by consideration of ASC and ANC constraints. Fully Constrained Least squares (FCLS) considers both the constraint whereas Non-negatively constrained least squares (NCLS) and Sum-to-one constrained least squares (SCLS) are the partial constrained methods in which SCLS imposes ASC and ignores ANC and NCLS imposes ANC and ignores ANC. Also, orthogonal subspace projection (OSP) is a method which ignores ASC and ANC.

The partially constrained methods (SCLS and NCLS) generally don't estimate targets effectively but can detect targets. Due to sum-to-one at ASC, SCLS cannot detect many target signatures usually in cases where we have many spectral bands being considered. But NCLS doesn't have such issues since it doesn't impose ASC, resulting in detection of many targets. Therefore, NCLS seems to be efficient over the detection of targets in comparison to SCLS.

Since, the above discussed least square methods comprises of imposed constraints based on abundance fractions ($\boldsymbol{\alpha}$). Thus, such methods are called target abundance-constrained approaches.

The above mentioned methods are not quite efficient for the detection of hotspot when its fraction is small; which is so because of the fact that hotspots are smaller in size when compared with the spatial resolution of MODIS images; most of the hotspots may be present partially within one or more pixel leading to mixed pixel issues. Therefore, detection of such smaller hotspots over a coarse resolution images are implied which can be attained by the aid of CEM approach since CEM is efficient over the detection of such smaller targets.

Constrained energy minimization (CEM)

Unlike the above methods, CEM is a target signature-constrained approach which constrains over the desired target signature instead of its abundance fraction. CEM can be described as an adaptive filter that minimizes the filter output energy while constraining a desired target signature by a specific gain [32]. Unlike the above mentioned abundance constrained approach which requires a prior knowledge about all the target class spectral signatures whereas CEM requires only the knowledge of desired signature.

Assume that we are given a finite set of observations $S = \{\mathbf{r}_1, \mathbf{r}_2, \ldots \mathbf{r}_N\}$ where $\mathbf{r}_i = (r_{i1}, r_{i2}, \ldots r_{iL})^T$ for $\mathbf{1} \leq \boldsymbol{i} \leq \boldsymbol{N}$ is an L-dimensional sample pixel vector. Let $\boldsymbol{d}$ denote the desired target spectral signature, which is known *a priori*. The objective is to design an FIR linear filter with L filter coefficients $\{w_1, w_2, \ldots w_L\}$ denoted by an L-dimensional vector $w = (w_1\ w_2\ \ldots\ w_L)^T$ that minimizes the filter output power in subject to the following constraint

$$\mathbf{d}^T \boldsymbol{w} = \sum_{l=1}^{L} \boldsymbol{d}_l \boldsymbol{w}_l = \mathbf{1} \tag{11}$$

Let y_i denote the output of the designed FIR filter resulting from the input r_i. Then y_i is

$$y_i = \sum_{l=1}^{L} \boldsymbol{w}_l \boldsymbol{r}_{il} = \mathbf{w}^T \boldsymbol{r}_i = \mathbf{r}_i^T \mathbf{w} \tag{12}$$

The average output power produced by the observation set S by using the above FIR filter with coefficient vector $\boldsymbol{w} = (w_1\ w_2 \ldots w_L)^T$ is specified by

$$\frac{1}{N}\sum_{i=1}^{N} y_i^2 = \frac{1}{N}\sum_{i=1}^{N}(r_i^T w)^T r_i^T w = w^T\left(\sum_{i=1}^{N} r_i r_i^T\right)w = w^T R_{LxL} w \qquad (13)$$

Where R_{LxL} = 1/N $[\sum_{i=1}^{N} r_i r_i^T]$ turns out to be the L x L *sample autocorrelation matrix* of S. Minimizing (xx) with the filter response constraint $d^T w = \sum_{l=1}^{L} d_l w_l = 1$ yields

$$\min_{w}\left\{\frac{1}{N}\left[\sum_{i=1}^{N} y_i^2\right]\right\} = \min_{w}\{w^T R_{LxL} w\} \quad \text{Subject to } d^T w = 1 \qquad (14)$$

The solution to (14) was shown in [54, 55] and called the CEM filter with the weight vector w^* given by

$$w^* = \frac{R_{LxL}^{-1} d}{d^T R_{LxL}^{-1} d} \quad w^* = \frac{R_L^{-1} d}{d^T R_{LxL}^{-1} d} \qquad (15)$$

The R_{LxL} in (15) is not necessarily full rank. Thus, calculating R_{LxL} can be cumbersome. It has been observed that CEM is very sensitive to the knowledge used for desired target as well as the noise [25]. As shown in experiments [32] the noise sensitivity is closely related to the rank used for the calculation of weight vector in (15). The rank of R_{LxL} determines the number of eigenvectors required for calculating R_{LxL}^{-1} and it is also closely related to the intrinsic dimensionality of a multi/hyper spectral image. In cases where R_{LxL} doesn't have full rank then the inverse of R_{LXL} can be computed by singular value decomposition such that $\hat{R}_{LxL} = \tilde{V}\Lambda\tilde{V}^T$ where $\tilde{V} = (\tilde{v_1}\ \tilde{v_2}\ \ldots \tilde{v_q})$ is an eigenmatrix, $\tilde{v_k}$ is the L-dimensional vector corresponding to the eigen value λ_k and Λ = diag$\{\lambda_1, \lambda_2, \ldots, \lambda_q\}$ is a diagonal matrix with eigenvalues as diagonal elements. Thus, by performing eigen-decomposition, the inverse of $\hat{R}_{LxL}$ can be found by $R_{LxL}^{-1} = \tilde{V}\Lambda^{-1}\tilde{V}^T$ [54]. But such decomposition requires a prior knowledge of knowing the number of eigenvectors. The deduction of optimal weight vector in (15) is elaborated in [55].

The application of CEM over classified hotspot image will yield a fractional image that comprises of fractions of hotspot present within a pixel. Thus, such image indicates the estimate of hotspot present within a region. But, in order to perform area estimation based on hotspot density, we perform segmentation by the aid of segmentation technique such as: Otsu multi-threshold method and cluster similarity measure based method called DBI using GA as its optimizing technique.

Step: 4 Hotspot prone zone segmentation

After obtaining hotspot fractional image from the previous step; it is important to segment the image into various zones based on hotspot subpixel fractional area. In this method, hotspot area are to be segmented into four zones. Thus, image segmentation technique is applied.

Image segmentation is the division of an image into various regions, each region will have a specific properties. Thus, segmentation is performed such that to group similar pixels together and these grouped pixels are segregated into various classes. Image segmentation can be performed by various threshold methods such as Otsu threshold, Maximum entropy based thresholding etc. as well as by clustering methods such as K-means.

In threshold method, we try to obtain a set of threshold levels (l_1, l_2, l_3....l_k) such that all pixel with $\mathbf{f(x,y) \in (l_i,\ldots l_{i+1})}$ where $i=0,1,\ldots k$ constitute the i-th region type. $f(x,y)$ represents the feature value at the (x,y) spatial coordinates of the pixel [58]. Thus, by using thresholding method, we obtain the threshold levels such that it segments the pixels into appropriate levels.

I. Otsu method

This method as proposed in [56] is to select an optimal threshold by the use of discriminant analysis over gray level histogram of the image to be segmented. In this method, the optimal threshold is chosen such that to partition of the pixels in an image into two distinct classes C_0 and C_1 at gray level t. Pixels with grey levels lesser/equal to t are into class C_0 (i.e., $C_0 = \{0,1,2,\ldots.t\}$) whereas pixels of greater grey levels than *t-level* are into C_1 (i.e., $C_1 = \{t+1,t+2, ,\ldots.L\}$). The threshold level is chosen based on *minimizing* the following discriminant criterion measures

$$\lambda = \frac{\sigma_B^2}{\sigma_w^2}, \qquad k = \frac{\sigma_T^2}{\sigma_w^2} \quad \text{and} \quad \eta = \frac{\sigma_B^2}{\sigma_T^2} \tag{16}$$

where σ_B^2 is the between-class variance

σ_w^2 are the with-in class variance

σ_T^2 are the total variance of levels.

Of all the above discriminant measures, η calculation is simplest [Otsu, 1979]. Thus, the optimal threshold gray level t^* is

$$t^* = Arg \min_{t \in L} \eta \tag{17}$$

Otsu method can be extended to multi-thresholding problems. For example, in the case of two thresholds, image gets segmented into three levels $1 \leq t_1 < t_2 < K$ such that minimization of discriminant measure is

$$t^* = Arg \min_{t_1, t_2 \in L} \eta \tag{18}$$

II. Segmentation – by clustering method

Segmentation can be reduced to the problem of clustering the pixels based on similarity measure within the cluster. Thus, we have performed segmentation based on cluster similarity measure called Davies-Bouldin index (DBI) using genetic algorithm. The advantage of GA-DBI is its assurance of providing global threshold levels even though in multi-threshold condition. But, Otsu fails over segmenting at optimal levels when multi-threshold of 3 or more levels are required and also, the non-requirement of histogram of source image for performing segmentation unlike Otsu multi-threshold.

GA-DBI clustering

GA-DBI is performed to classify (i.e., segment [57]) an image into its feature classes by performing GA operations using Davies-Bouldin index (DBI) as its fitness function [15]. This fitness value is used as a guide to the stochastic selection of chromosomes which are then considered for further operation: crossover and mutation. Crossover generates new chromosome by performing single point crossover over two or more selected parents [18]. Mutation acts by randomly selecting genes to be altered thereby avoiding the persistence of local-optimal solutions and thereby improving the diversity within population.

Step 1: String Representation:

In GA-DBI, the chromosomes were made up of grayscale values of our image to be segmented and the length of chromosome is equivalent to the number of clusters (i.e., number of threshold levels) as each genes of chromosome refers to the centre of cluster [15].

Step 2: Population Initialization:

For each string *i* in the population (i=1,…,P where P is the size of population), *i* refers to the value of cluster centre. Since, the number of cluster is known prior, the length of chromosome is fixed as each chromosome comprises of n genes (*n* refers to number of clusters) [15]. These cluster centres are chosen randomly from the data set as well as distributed randomly in the chromosomes.

Step 3: Fitness Computation:

The fitness of a chromosome is computed using Davies-Bouldin index. This index is to group similar pixels within in an image based on the ratio of intra and inter-cluster distance.

$$\mu_{kn} = \begin{Bmatrix} 1; \|x_n - u_k\| \le \|x_n - u_j\| \\ 0; \quad otherwise \end{Bmatrix} 1 \le k, j \le K; j \ne k; 1 \le n \le N \qquad (19)$$

x_n = pixel *n* with grey values *x*.

N = Total number of pixels.

μ_{kn} = indicator variable of each pixel belonging to cluster k.

u_k = centre of k^{th} cluster

$$v_k = \frac{\sum_{n=1}^{M} (\mu_{kn}) x_n}{\sum_{n=1}^{M} \mu_{kn}} \qquad (20)$$

Where, v_k = average value of each cluster

$$S_k = \frac{1}{|X_k|} \left(\sum_{i=1}^{|X_k|} \|x_i - v_k\|^2 \right)^{1/2} \qquad (21)$$

Where, X_k = Number of pixels belonging to k^{th} cluster

S_k = standard deviation of the pixels in k^{th} cluster

$$d_{k,j} = \left\| v_k - v_j \right\|_2 \tag{22}$$

Where, d_{kj} = Euclidean distance between the k^{th} and j^{th} centroids.

$$R_k = \max_{j \neq k} \left\{ \frac{S_k + S_j}{d_{k,j}} \right\} \tag{23}$$

Where, R_k is the maximum value of the ratio between inter and intra-cluster distance

$$DB = \frac{1}{K} \sum_{k=1}^{K} R_{k,i} \tag{24}$$

The DBI value is the average value of R for all cluster

$$DBI = \min \left\{ \frac{1}{DB} \right\} \tag{25}$$

The aim of the method is to minimize the DBI. In other words, the cluster which is formed is equivalent to the cluster with smallest intra-cluster and the largest inter-cluster distance. After calculating DBI for each chromosome from the population, those chromosomes which have minimal DBI value will be called as the best chromosome. For each generation, best chromosomes are obtained and they are compared with the previous generation (iteration). The termination condition is attained either if the differences between these two chromosomes are lesser than a pre-defined threshold value or it has reached the maximum iteration.

Thus, after the termination of algorithm, an elite chromosome is given which comprises of those cluster centres which have been very closer to its mean value when compared between the distance of cluster centres and their respective means found in other chromosomes. The entire flow is depicted in figure: 3.9.

In cases for performing Image segmentation using GA-DBI, the chromosomes are made from the population which comprises of grayscale values of the image to be segmented and the length of our chromosome is equivalent to the number of threshold levels. Thus, after optimizing the fitness function with the aid of various genetic algorithm operators such as crossover, selection and mutation; the resulting optimal set of grayscale values indicate the threshold levels by which we segment the image into various regions.

The entire flow chart of subpixel classification of hotspot for area estimation is depicted in fig. 3.10.

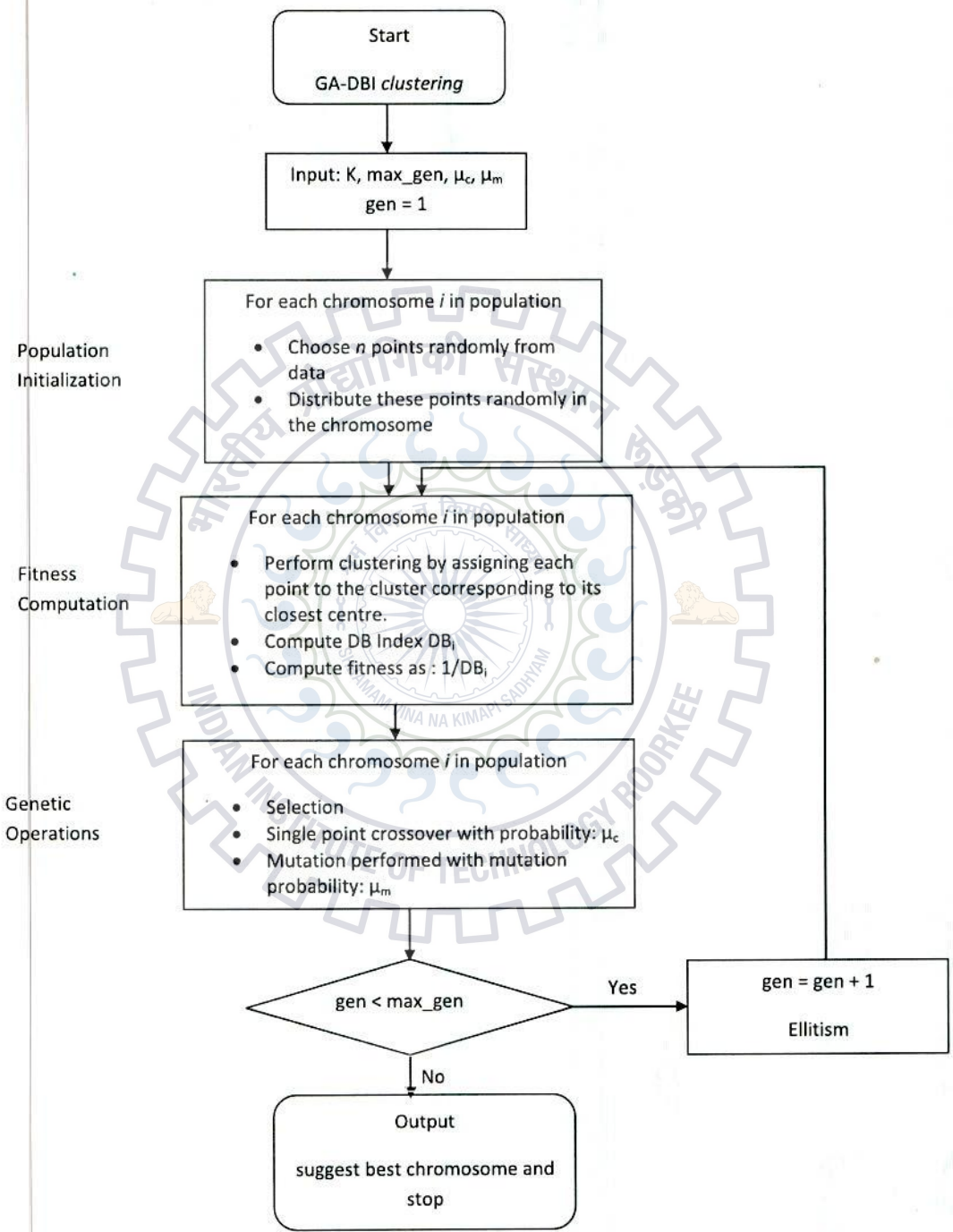

Figure 3.9 Flow chart of GA-DBI clustering

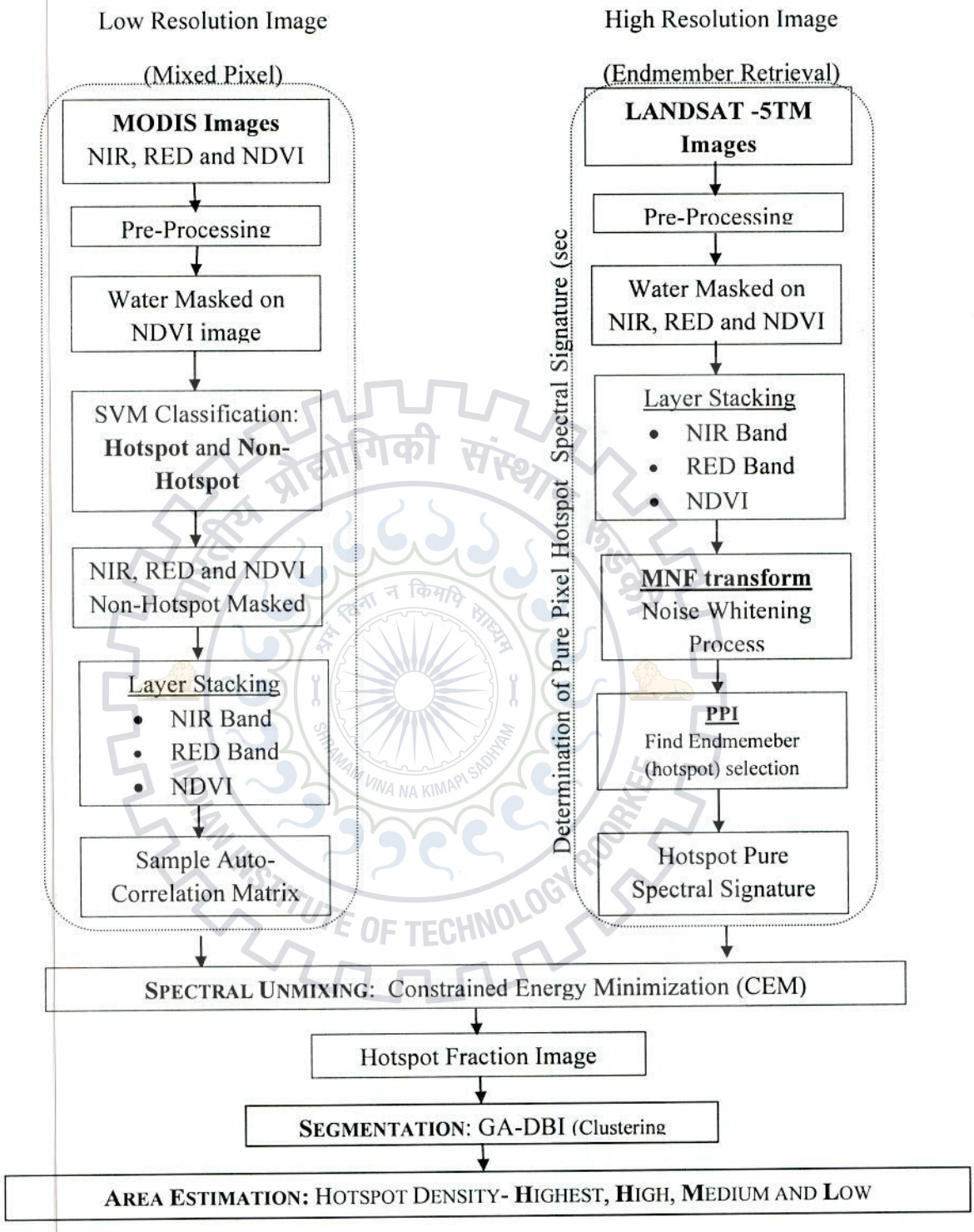

Figure 3.10 Flow chart for subpixel classification of hotspots for area estimation

CHAPTER 4
METHODOLOGY

In this chapter, the methodology devised for per pixel spectral-based hotspot classification and subpixel spectral-based classification of hotspots for area estimation are elaborated.

4.1 Methodology for per pixel spectral-based hotspot classification

The detection of hotspots and non-hotspots were carried using satellite Images. Optical datasets such as Landsat-5TM, MODIS and NOAA/AVHRR are used for performing per-pixel spectral based classification; such classification is carried by using various classification techniques as discussed in section 3.5 and the entire flow is depicted in fig. 3.8. Also, the corresponding dataset MODIS, LANDSAT-5TM and NOAA/AVHRR are identified as: MOD1, LST1 and AVH1. The methodology for performing per pixel spectral-based classification for hotspot detection is as follows:

Step 1: As discussed in section 3.3, the optical images that are available in sinusoidal projection are converted to geographic lat/lon (WGS84).

Step 2: NDVI image is then computed from the available red and NIR bands of the preprocessed optical images using the equation (1) mentioned in section 3.4.

Step 3: The obtained NDVI image is then classified into hotspot and non-hotspot classes using different classification techniques as mentioned in section 3.5.

Step 4: The classified pixels are assessed by test data set using the metrics HDA and FAR as mention in equation (7) and (8) respectively of section 3.6. These were done to measure the accuracy of classification algorithms over segregating pixels based on its class feature: hotspot and non-hotspot.


भारतीय प्रौद्योगिकी संस्थान रुड़की
श्रम विना न किमपि साध्यम
SHRAMAM VINA NA KIMAPI SADHYAM
INDIAN INSTITUTE OF TECHNOLOGY ROORKEE

4.2 Methodology for subpixel spectral-based classification of hotspots for area estimation

This task focuses on estimating the area coverage of hotspot regions of Jharia at subpixel scale with the first two MODIS surface reflectance bands along with its NDVI image. Though the spatial resolution of MODIS is 250m but detection of hotspot at such moderate spatial resolution could be cumbersome. Due to the fact that hotspot may not lie entirely on a single pixel but be present partially in the pixel. Thus, it is not viable to estimate the hotspots with better accuracy using the pixel level information of MODIS images. Therefore, the work utilizes a high resolution LANDSAT-5TM image of Jharia region for identifying the present pixel's spectral signature. Also, the LANDSAT-5TM dataset used for this study is identified as (Data_Id: LST2) and our test MODIS dataset is MOD3 whereas for validation we have used MOD2 and MOD4.

The algorithm is primarily of two steps:

1. Determination of present hotspot spectral signature from high resolution data-LANDSAT-5TM dataset (LST2).
2. Application of constrained subpixel spectral target detection on low resolution MODIS image to estimate the actual fraction of hotspot in mixed pixel spectrum.

After obtaining the fraction image of spatial presence of hotspots; Area estimation of hotspots is done using image segmentation technique such that the hotspot regions can be segmented based on the dense presence of hotspots. The entire flow of work is depicted as flow chart in fig 3.10.

4.2.1 Determination of purest hotspot spectral signature

The flow chart at fig. 3.10 indicates the entire flow during the process of obtaining purest hotspot spectral signature from Landsat-5TM image of Jharia region. These steps are elaborated in the following steps.

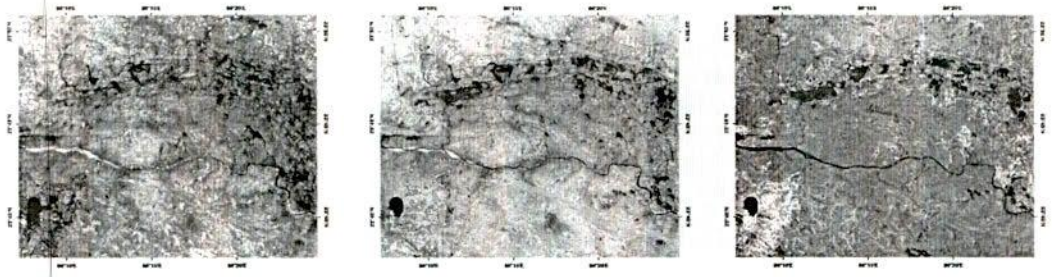

a. RED band Image b. NIR band Image c. NDVI Image

Figure 4.1 Landsat-5TM Preprocessed Image of Jharia region (a). Band-3 (RED) Image (b). Band-4 (NIR) Image (c). NDVI Image.

Step 1: Landsat-5TM (LST2) image is available as pre-processed; thus, only projection conversion from sinusoidal to geo Lat/Lon (WGS-84) is performed. The Preprocessed image of red and NIR bands are shown in fig. 4.1(a) and 1(b) respectively.

Step 2: Band-3 (red), band-4 (NIR) and NDVI (calculated from equation (1) in section 3.4); they are stacked in the sequence: band-3, band-4 and NDVI. The corresponding NDVI image is shown in fig.4.1(c). In the further steps the stacked image will be considered as a single image i.e., as a multiband image.

Step 3: The minimum noise fraction (MNF) transform is performed over the stacked images for noise removal which is a pre-requisite step for PPI.

Step 4: Pixel purity index algorithm is applied over the MNF transformed image in order to obtain the pure spectral signature of hotspot by projecting the MNF image onto a random unit vectors called skewers such that the cumulative records of extreme pixels obtained from each projection is noted. Those pixels with such extremity scores are considered to be the pixel purity index. Those extreme-score pixels highlighted over the PPI process are shown in fig. 4.2(a). The PPI algorithm is performed as described in *step: 2* of section 3.7.

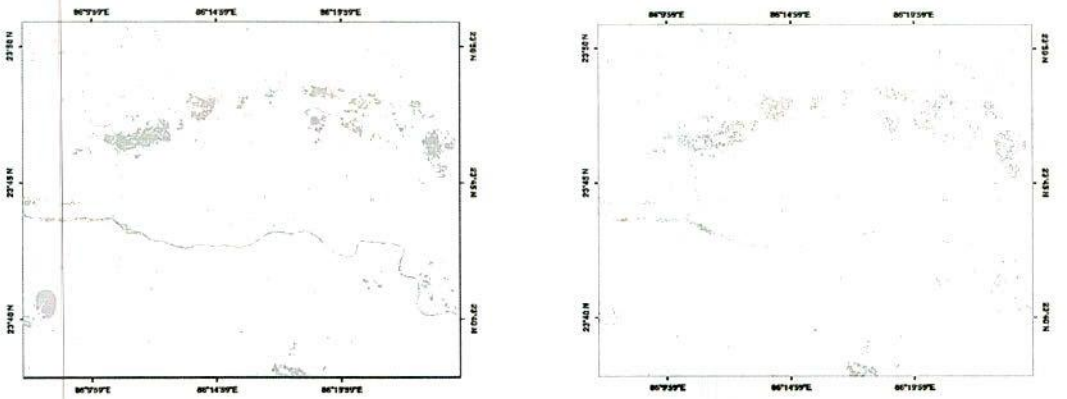

a. PPI Image b. PPI Image (Water Masked)

Figure 4.2 Pixel Purity Index applied over the MNF transformed image of Landsat-5TM. (a). PPI Image. (b). PPI image where water pixels were excluded since it makes cumbersome over the detection of hotspots.

Figure 4.3 SVM classified Image of Landsat-5TM image over our study region. The BLUE, RED and GREEN color denotes Water, Hotspot and Non-Hotspot regions respectively.

Step 5: The above obtained pixels are compared against the spectral signature of hotspot whichever is found to be closer is identified as the purest pixel. Thus, the obtained purest spectral signature of hotspot will be used as the desired *target spectral signature* for the CEM method to be discussed below. During this process, water pixels have been explicitly excluded by masking them since the presence of water pixels created difficulties over obtaining the purest pixel spectra of hotspot. This masking is performed with the aid of the classified image over the same study region such that the entire pixels were classified into

hotspot, non-hotspot and water regions as shown in fig. 4.3. These water pixels were omitted during the PPI process. This classification was carried with an intention to obtain around 90% accuracy (our classified image is of *91.4% accuracy*) using SVM classification technique (as discussed in *step: 1* of section 3.7.). The water masked PPI image is shown in fig. 4.2(b).

4.2.2 Estimation of hotspot area fraction over mixed pixel using constrained subpixel target detection method

The left hand flow of steps as depicted in flow chart at fig.3.10 indicates the entire flow during the process of obtaining hotspot area fraction image using CEM as discussed in the below steps.

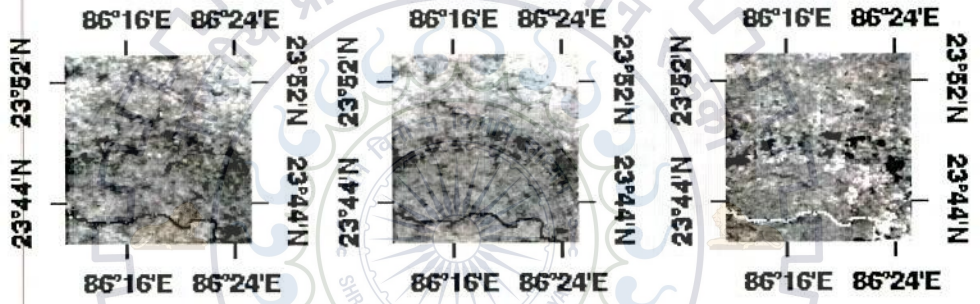

a. RED Band Image b. NIR Band Image c. NDVI Image

Figure 4.4 Preprocessed MODIS Image- a. RED, b. NIR and c. NDVI Band Image

Step 1: Pre-processing of MODIS image is carried as discussed in section 3.4. The red, NIR pre-processed image are shown in fig. 4.4 (a and b).

Step 2: Water regions are masked such that all water pixels are excluded from the computation as their presence hinders over the estimation of hotspots. The water masked image of NDVI preprocessed image are shown in fig. 4.4c.

Step 3: Supervised classification using SVM classifier is performed over the NDVI water masked image such that the resultant classified image comprises of only two classes: hotspot and non-hotspot. The classification is performed with intent to obtain above 90% accuracy over the classification of the image into hotspot and non-hotspot. The water masked NDVI image as well as its corresponding classified Image are shown in fig. 4.5.

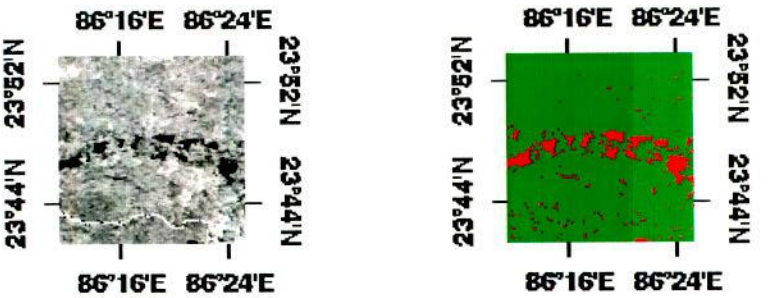

a. NDVI water masked Image

b. Classified Image

Figure 4.5 Per-Pixel based classification of MODIS image. (a).NDVI Image – water pixels were explicitly modified to have its DN value ranging within the non-hotspot class range. (b). Supervised classification was performed by SVM technique such that the pixels are classified to fall into either hotspot or non-hotspot class. RED refers Hotspot class and GREEN refers Non-Hotspot class.

Step 4: The Layer stacking of NIR, RED and NDVI is performed such that the hotspot pixels are only considered meaning that non-hotspot pixels are masked and only hotspot pixels are retained. This stacked image will be considered as a single image cube comprising of 3-layers i.e., as a multi-band image.

Step 5: Sample Auto-correlation matrix R_{LxL} [i.e., $R_{LxL} = 1/N \left(\sum_{i=1}^{N} r_i r_i^T\right)$ where L=number of images within the stack which is 3 in our case] is computed from the stacked images which will be an input variable for constrained energy minimization (CEM).

Step 6: Subpixel target detection is performed by CEM where sample auto correlation matrix and Hotspot pure spectral signature (from section *4.2.1*) are used as its input variable. The reason for consideration of CEM is because of the following reason: CEM is found to be very effective in the detection of small targets, as in our case for the detection of those hotspots which are minor in size in comparison with the spatial resolution of MODIS. Also, CEM is found to be a very practical approach as it requires only the prior knowledge about knowing only the desired target spectral signature (i.e., hotspot) unlike other techniques such as FCFS, NCLS which requires the knowledge spectral signature of all classes. As the final step, the optimal weight vector is computed by optimizing R_{LxL} with the unity constraint as shown in equation (15) under section 3.7.

Step 7: The output of CEM is a fraction image where each pixel of the fraction image quantifies the density of hotspots present within the pixel while minimizing the presence of

other classes. Also, CEM fractional values not necessarily bound between 0 and 1. Thus, in order to bound the fraction of hotspot; negative fractions are retained as zero and fractions above one as one. It is done with an intuition that the pixels of fraction image quantifies the presence of hotspots; thus negative and above one fractional values are bounded to zero and one respectively.

Step 8: The image obtained as the output of CEM is a fractional image where the fractional value of each pixel indicates the amount of hotspot comprised within a pixel.

Step 9: In order to estimate the area into various classes based on hotspot density; the above derived fraction image where segmented using the various segmentation techniques.

Step 10: The segmentation technique GA based DBI were performed over the fraction image in order to segment the image into four classes: highest, high, medium and low as per the hotspot density. For the implementation of GA-DBI, the chromosomes are made from the population which comprises of grayscale values of our image (i.e., fraction image obtained from CEM) and the length of our chromosome is equivalent to the number of threshold levels. Thus, after optimizing the fitness function with our fraction image as input, the resulting optimal set of grayscale values indicate the threshold levels by which we segment the image such that each segment is treated as various classes based on the hotspot density. The performance of segmented image was verified with Otsu multi-threshold method. The detailed description about GA-DBI and Otsu multi-threshold are briefed in *step: 4* of section 3.7.

CHAPTER 5

RESULTS AND DISCUSSION

In this chapter the results obtained while performing per pixel hotspot classification and area estimation of hotspot coverage by subpixel classification are discussed in detail.

5.1 Results of per pixel classification for detection of hotspots

The detection of hotspot over optical dataset: NOAA/AVHRR, MODIS and Landsat-5TM is carried by the aid of classification such as supervised classification: Minimum (mean) distance classifier, Parallelepiped, GA-KMI clustering and unsupervised classification: ISODATA and K-means. The classified images over the datasets mentioned in section 3.4 are shown in this chapter and its corresponding HDA and FAR are discussed. The datasets respective data_id's are: AVH1, MOD1, LST1.

NDVI image obtained from NOAA/AVHRR is shown in fig. 5.1(a). This NDVI image is classified using different supervised and unsupervised classifiers. The classified images contains two feature classes: hotpost and non-hotspot pixels as depicted in fig. 5.1(b-f) for different classifiers. The calculated HDA and FAR are shown in table: 5.1. It is noticable that parallelepiped assigns certain pixels into an unknown classifier. Similarly, MODIS and Landsat 5TM NDVI images are classified into target classes: hotspot and non-hotspot, and the classified images are shown in fig. 5.2(b-f) and fig. 5.3(b-f) respectively.

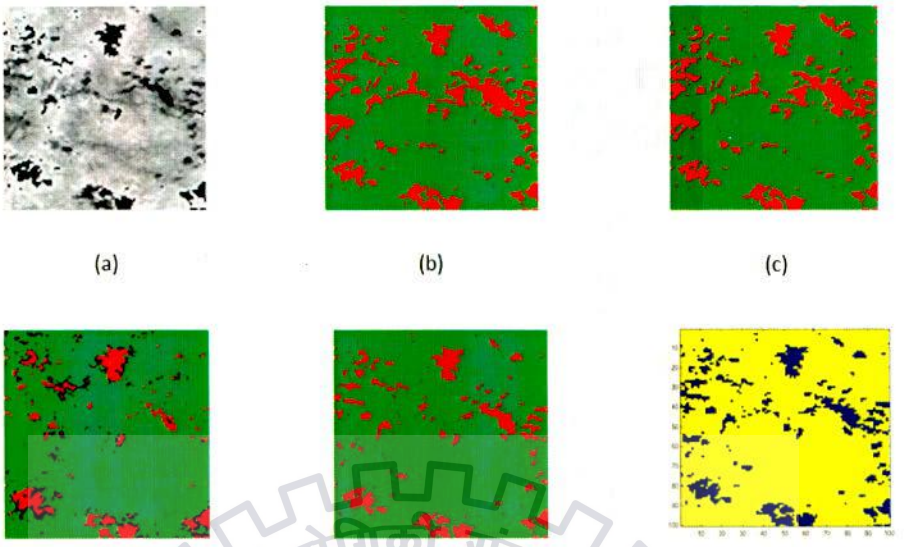

Figure 5.1 Classified Image of NOAA/AVHRR .Color code: (RED/BLUE)-Hotspot, (Yellow/Green)-NonHotspot and Black-Non-classified. (a) NDVI , (b) ISODATA, (c) K-means, (d) parallelepiped, (e) minimum distance and (f) GA-KMI clustering.

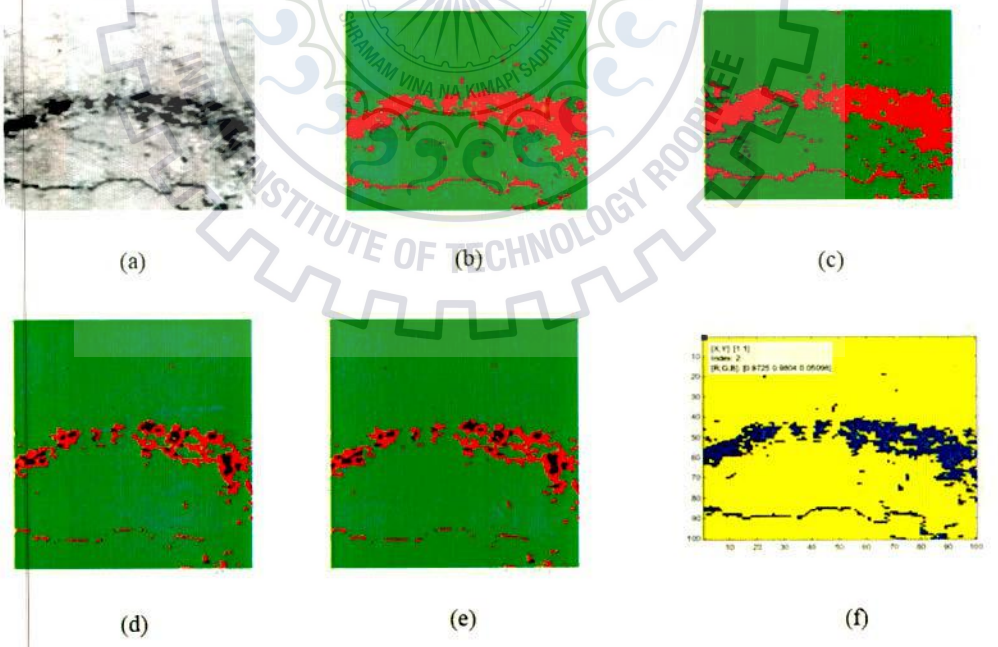

Figure 5.2 Classified Image of MODIS. Color code: (RED/BLUE)-Hotspot, (Yellow/Green)-NonHotspot and Black-Non-classified. (a) NDVI , (b) ISODATA, (c) K-means, (d) parallelepiped, (e) minimum distance and (f) GA-KMI clustering.

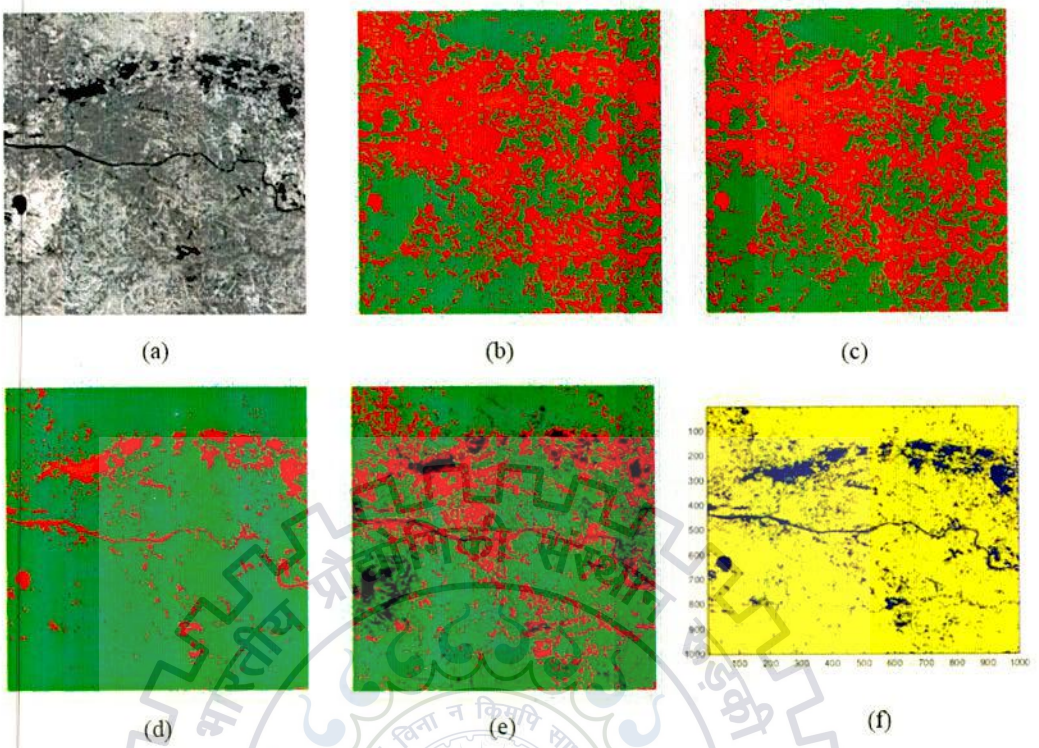

Figure 5.3 Classified Image of LANDSAT-5 TM. Color code: (RED/BLUE)-Hotspot, (Yellow/Green)-NonHotspot and Black-Non-classified. (a) NDVI , (b) ISODATA, (c) K-means, (d) minimum distance, (e) parallelepiped and (f) GA-KMI clustering.

Table 5.1 HDA and FAR for different classifiers on satellite images

Satellite Data	Supervised classification						Unsupervised classification			
	Minimum Distance (%)		Parallelepiped (%)		GA-KMI (%)		ISODATA (%)		K-Means (%)	
	HDA	FAR	HDA	FAR	HDA	FAR	HDA	FAR	HDA	FAR
MODIS (MOD1)	70	70	70	70	81	11	92	20	89	17
LANDSAT 5TM (LST1)	67	18	68	33	61	16	86	56	86	56
NOVAA/AVHRR (AVH1)	5	75	32	8	57	13	79	19	75	18

From table 5.1, It is observed that classified images from MODIS data indicates that the best classified image obtained are as that of GA-KMI having HDA as 81 % and FAR as 11% while ISODATA has HDA as 92% and FAR as 20% while others are having high FAR and low HDA comparatively.

LANDSAT 5 TM classified images shows that out of all classifiers K-means and parallelpiped has high HDA but low FAR while GA-KMI has a high HDA and high FAR which indicates that GA-KMI yeild better performance for detecting hotspots.

Whereas, NOAA/AVHRR indicates that ISODATA and K-means have higher HDA of 75% and 79% but has lower FAR whence GA-KMI has an average performance comparatively.

Overall, it shows that GA-KMI has higher HDA and FAR bounded within very lower upper bound. Thus, confirms that GA-KMI has higher performance over the other techniques .

5.2 Results of hotspot area estimation by sub pixel classification

We have performed subpixel spectral detection of target using CEM for the estimation of hotspot over MODIS image with the aid of High resolution (Landsat-5TM) image for the detection of pure hotspot spectral signature.

As explained in the previous section, finding of pure spectral signature of hotspot pixel using LST2 (i.e., Landsat-5TM image) is initially performed and pixel based classification over MODIS and Landsat-5TM image are done; such that the Landsat classified image is used for the detection of hotspot pixels which will be considered for obtaining hotspot spectral signature using PPI algorithm such that the search of pure pixel within the hotspot target class (hotspot classified image) gives an assurance of such pixels to be more viable as pure hotspot pixel; such pixels are then compared with the target spectra of hotspot class (as a final step of PPI algorithm). Thus, SVM classification is performed on LST2 and the obtained classified image confusion matrix is as shown in Landsat-5TM column in table 5.2.


भारतीय प्रौद्योगिकी संस्थान रुड़की
श्रम विना न किमपि साध्यम्
SHRAMAM VINA NA KIMAPI SADHYAM
INDIAN INSTITUTE OF TECHNOLOGY ROORKEE

Table 5.2 Confuse matrix and Kappa value of classes: Hotspot, Non-Hotspot and Water (considered only for LANDSAT-5TM dataset) region over MODIS and LANDSAT-5TM images.

	LANDSAT-5TM (LST-2) in %				**MODIS (MOD3)** in %		
	Hotspot	Non-Hotspot	Water	Producer Accuracy	Hotspot	Non-Hotspot	Producer Accuracy
Hotspot	65.06	0.00	2.02	65.06	77.22	0.00	77.22
Non-Hotspot	20.48	100.00	0.00	100.00	22.78	100.00	100.00
Water	14.46	0.00	97.98	97.98	NOT PERFORMED		
User Accuracy	96.43	91.28	88.99		100.00	85.37	
Kappa Value	0.8595				0.7946		
Overall Accuracy	91.389				90.217		

Also, our intention is to refine the estimate of hotspots present within a hotspot detected pixel of MODIS image. Thus, subpixel target detection is performed over the per-pixel spectral-based classified image (classification done by SVM classifier). Thus, such classification was done with an intention to obtain higher accuracy (above 90%) and kappa value as shown in table MODIS column in 5.2.

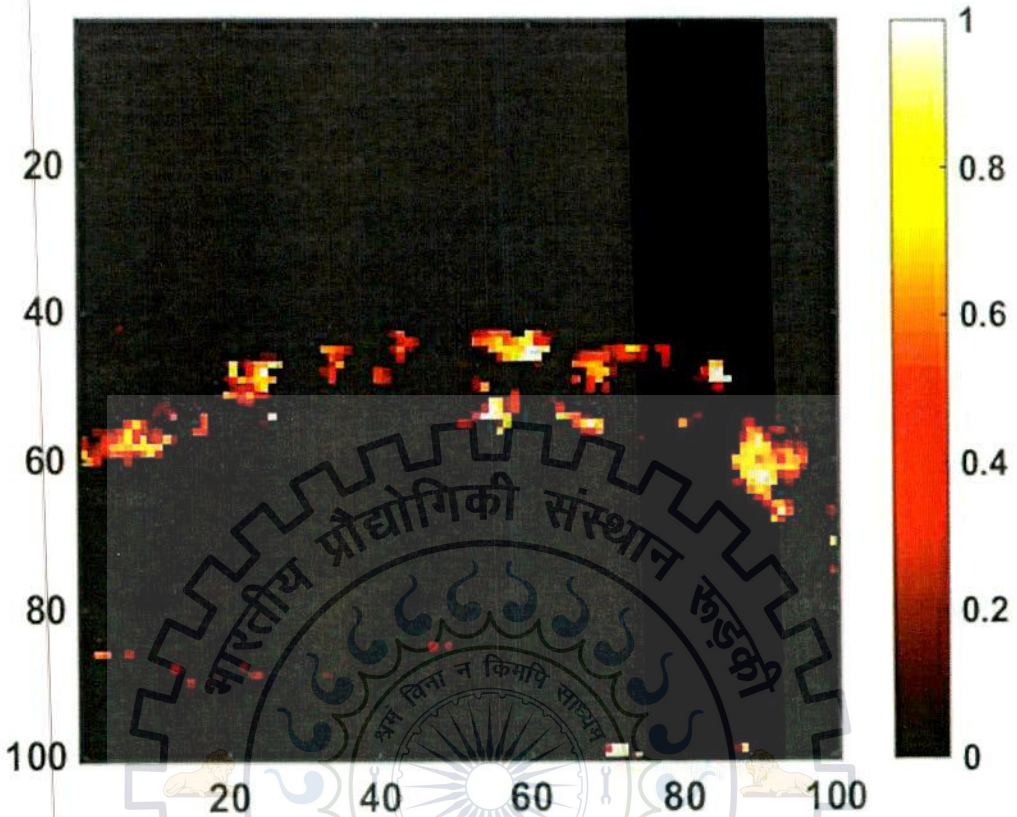

Figure 5.4 CEM Fraction Image. Indicates the presence of Hotspot within each pixel varying from 0 to 1 (0 refers absence of hotspot and 1 refers enriched presence of hotspot).

These refined hotspot pixels spectral values were considered for performing target detection at subpixel level using CEM such that the obtained output image indicates the fraction of hotspot present within the per-pixel classified hotspot pixel as shown in fig. 5.4. This fractional image is segmented into various classes: Highest, High, Medium and Low based on density of hotspot coverage; using GA based DBI. The segmentation of GA-DBI is compared with Otsu multi-threshold method. The segmented image by GA-DBI and Otsu Multi-Threshold are shown respectively in figure 5.5 and 5.6.

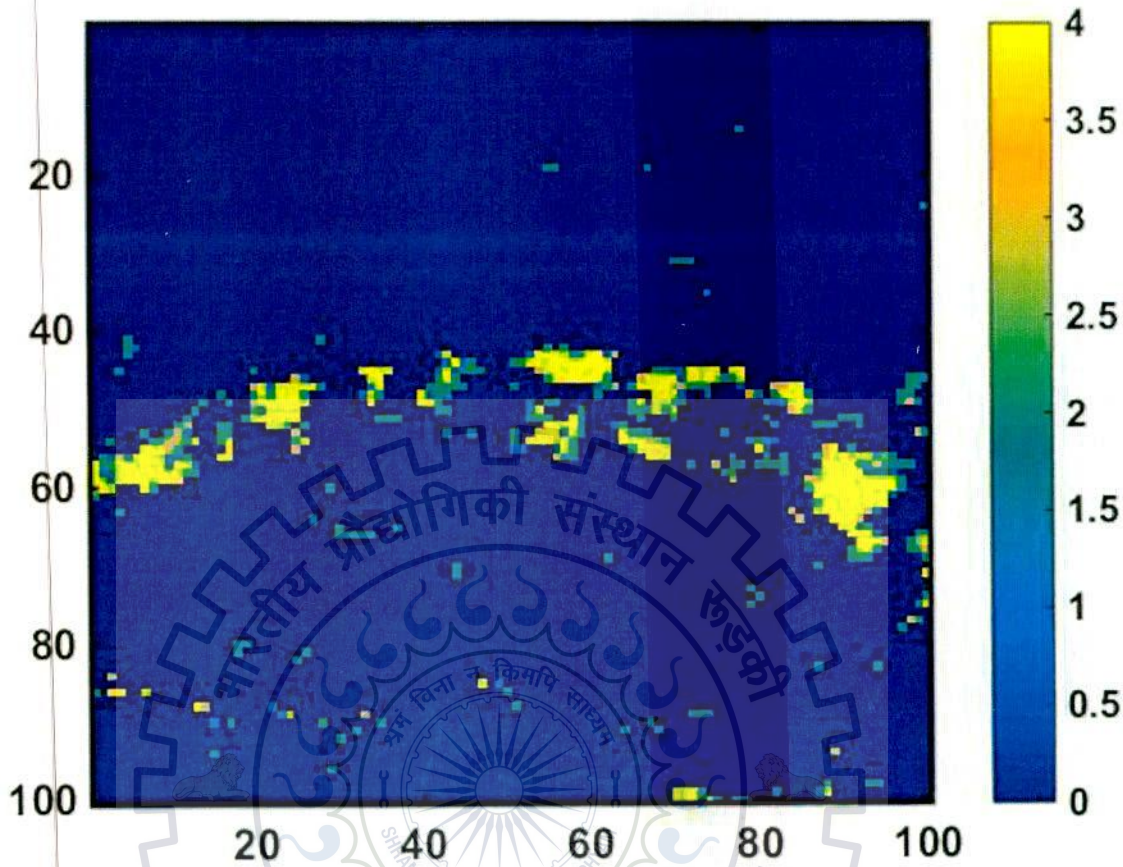

Figure 5.5 CEM fractional hotspots are segmented into various classes by GA-DBI: Low (0-1), Medium (1-2), High (2-3) and highest (3-4).

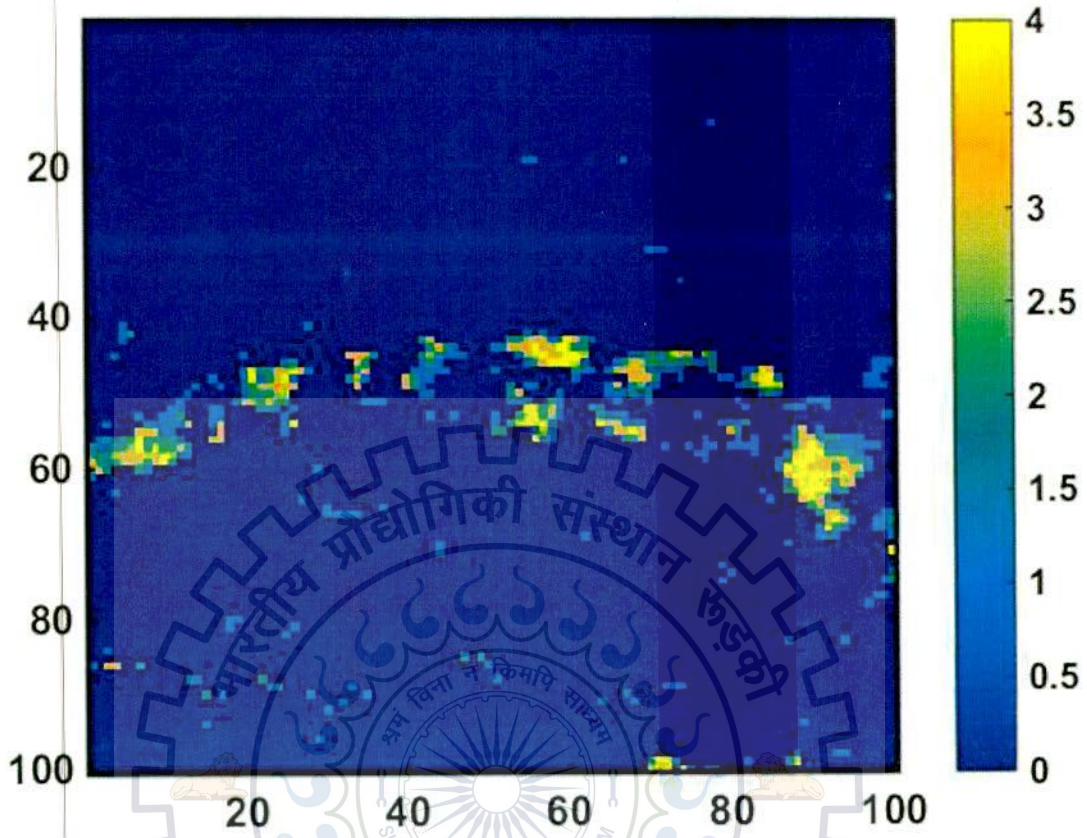

Figure 5.6 CEM fractional hotspots are segmented into various classes by Otsu Multi-threshold: Low (0-1), Medium (1-2), High (2-3) and highest (3-4).

The area estimation of hotspot at various segmented levels is shown in table 5.3.

Table 5.3 Lists Hotspot density coverage in Km^2 for various classes over different temporal dataset MOD3, MOD4 and MOD2 are acquainted on 14-March-2015, 30-March-2015 and 23-March-2012 respectively.

MODIS dataset	Segmentation / Hotspot Area Estimation	HIGHEST	HIGH	MEDIUM	LOW	Total Area
MOD3	Otsu Method	4.2615	4.2806	2.1894	0.3549	11.086
	GA-DBI	10.099	0.27762	0.0332	0.6768	
MOD4	Otsu Method	4.039	3.9507	2.468	0.4634	10.921
	GA-DBI	8.6073	0.6233	0.01672	1.6737	
MOD2	Otsu Method	4.1601	2.5212	1.5064	0.2511	8.4387
	GA-DBI	7.6205	0.3239	0.1115	0.3829	

As mentioned in *step: 4* in section 3.7, Otsu multi-threshold is not optimal when it comes to three or higher levels of threshold. Thus, we have used GA-DBI for our case: segmenting fractional image into four classes (i.e., 3-level thresholding). Since, GA-DBI segmentation is performed by GA which is a heuristic method that promises in leading to global optimization. As shown in table 5.3, GA-DBI indicates that the level bound for "Highest" segment is larger when compared with "Highest" segment of Otsu whereas other segments are tightly bounded in comparison to Otsu.

MOD4 and MOD2 datasets of 30-March-2015 and 23-March-2012 respectively; have been used for validation of our hotspot area estimation by subpixel analysis with the dataset MOD3 (i.e., data acquaintance date is 14-March-2015). For segment comparison purpose, we have considered segments generated by GA-DBI.

When MOD3 is compared with a weekly varied temporal data (i.e., MOD4); it indicates that the hotspot area coverage variation is in negligible value especially among the respective segments. Also, the total area hotspot coverage between them is of 0.165 Km^2 variance.

In the need of validating MOD3 for yearly variation, MOD2 dataset is used and it is observed that the hotspot density over various segments indicates that there is a 1 Km^2 increase in denser hotspot, 0.3 Km^2 increase in high density hotspot coverage, 0.1 Km^2 variation in medium hotspot density segment and almost 1.29 km^2 low denser hotspot has been increased within the span of 2012 to 2015.

CHAPTER 6

CONCLUSION AND FUTURE SCOPE

6.1 CONCLUSION

The detection of hotspots using various supervised and unsupervised classification on per-pixel spectral based classification result shows that GA-KMI has higher performance over the other techniques and it is so because of unbounded space over the range for choosing the optimal value compared to the others as they are bounded to choose within a limited search space. In other words, GA-KMI has wider scope to find the correct hypothesis (optimal center) since the search space of hypothesis is relaxed and such relaxation is attained by the choice of GA parameters such as: Population size, number of generation and GA operators: crossover and mutation.

Also, regarding the satellite dataset, the per-pixel spectral based classifier indicates that MODIS can be used for the detection of hotspot since it has a good trade-off over detection of hotspot with good accuracy (81%- HDA, 11%-FAR: attained by GA-KMI clustering) and good temporal resolution. But due to mixed pixel issues and also the smaller in size of hotspot, the detected hotspot by per-pixel classifier cannot lead an accurate estimation of hotspot coverage.

Thus area estimation of hotspot coverage has been performed by refining the hotspot detected by per-pixel classifier over MODIS dataset. This refinement of per-pixel detected hotspot is done by the application of subpixel classification using target constrained approach called CEM. Since, it is quite efficient in the detection of smaller targets; thus, hotspot coverage area estimation is performed using CEM. Also, the resultant hotspot area coverage estimation has been validated with dataset of weekly and yearly variation, we find that hotspot of 0.165 Km^2 of variation been observed within a week and 2.647 Km^2 of increased Hotspot coverage is observed over a period of two years.

6.2 FUTURE SCOPE

Hotspot Monitoring can be further done by the aid of SAR images as one can take advantage of its microwave application and its higher spatial resolution. Also, as a better trade-off of spatial and temporal resolution, data fusion of various sensors can be utilized since data fusion among

various sensors of different time series dataset can aid for creating up a hotspot monitoring system.

Also, from the aspect of the study discussed on subpixel analysis by target constrained approach –CEM; have shown that only one target can be detected simultaneously but this could be extended further to detect more than one class of target like vegetation, water, bare soil classes etc., by obtaining optimal weight vector for each targets by constraining over all target signature rather than a single target signature as shown in equation (11) in section 3.7. Also, the advantage of CEM is it can be implied in real-time processing and can be used to detect small targets efficiently; thus, CEM can be utilized for tasks such as crop identification; which requires recognition of target of smaller size but with an explicit constraint that is, its spectral characteristic should be very similar to the desired target signature knowledge within the mixed pixel.

REFERENCES

1. Stracher B.G, Prakash A, Sokol E.V, "Coal and Peat Fires: A Global Perspective: Volume 3: Case Studies - Coal Fires", vol 3, 1st ed., Elsevier Science, 2014.
2. V Jyothi,B Rajesh Kumar, P Krishna Rao, D V Rama Koti Reddy "Image fusion using evolutionary algorithm (GA)" Int. J. Comp. Tech. Appl., Vol 2 (2), 322-326.
3. Aqeel Mumtaz, Abdul Majid, Adeel Mumtaz "Genetic Algorithms and its Application to Image Fusion" IEEE-ICET 2008.
4. T.Ahmed, D. Singh, S. Gupta and B. Raman and An efficient application of fusion approach for hot spot detection with MODIS and PALSAR-1 data, Geocarto Intl., 2015.
5. T. Ahmed, D. Singh, S. Gupta and R. Balasubramanian, "Particle Swarm Optimization Based Fusion of MODIS and PALSAR Images for Hotspot Detection," Int. Conference on Microwave and Photonics (ICMAP), Dhanbad, India, 13th-15th December 2013.
6. T. Ahmed, D. Singh, S. Gupta and R. Balasubramanian, "Particle Swarm Optimization Based Fusion of MODIS and PALSAR Images for Hotspot Detection," Int. Conference on Microwave and Photonics (ICMAP), Dhanbad, India, 13th-15th December 2013.
7. Bushra N. Kayani, Anwar Majeed Mirza, Ajmal Bangash, Haroon Iftikhar "pixel & feature level Multiresolution image fusion based on fuzzy logic" Innovations and Advanced Techniques in Computer and Information Sciences and Engineering, 129–132, Springer 2007.
8. Sicong Liu a, Peijun Du a, Paolo Gambab, Junshi Xia a "Fusion of Difference Images for Change Detection in Urban Areas" Joint Urban Remote Sensing Event April 11-13, 2011.
9. R. S. Gautam, D. Singh, A. Mittal, "A fuzzy logic approach to detect hotspots with NOAA/AVHRR image using multi-channel information fusion technique" International Journal of Signal Image and Video Processing, Springer, 2007.
10. Chen Y. and Wang J. Z., "Support vector learning for fuzzy rule-based classification systems," IEEE Transactions on Fuzzy Systems, vol. 11, no. 6, 2003, pp. 716–728.
11. Gunn S. R., "Support Vector Machines for classification and regression," Technical Report, Faculty of Engineering, Science and Mathematics, School of Electronics and Computer Science, University Of Southampton, 1998.


भारतीय प्रौद्योगिकी संस्थान रुड़की
श्रमं विना न किमपि साध्यम्
SHRAMAM VINA NA KIMAPI SADHYAM
INDIAN INSTITUTE OF TECHNOLOGY ROORKEE

12. Hsu C. -W., Chang C. -C., and Lin C. -J., "A practical guide to support vector classification," Technical report, Department of Computer Science and Information Engineering, National Taiwan University, Taipei, 2003.
13. R. Agarwal, D. Singh, D. S. Chauhan and K. P. Singh, "Detection of coal mine fires in the Jharia coal field using NOAA /AVHRR data", J. Geophys. Eng. 3, pp 212–218, 2006.
14. R. S. Gautam, D. Singh, A. Mittal, and Sajin P "Application of SVM on satellite images to detect hotspots in Jharia coal field region of India" Advances in Space Research, Elsevier, 2007.
15. S Bandyopadhyay and U Maulik,"Genetic clustering for automatic evolution of clusters and application to image classification", Pattern Recognit., vol. 35, pp. 1197–1208, 2002.
16. Y. F. Yang, P. Lohmann, and C. Heipke, "Genetic algorithms for the unsupervised classification of satellite images," in Proceedings of the Symposium of ISPRS Commission III, Photogrammetric Computer Vision (PCV '06), vol. 36, pp. 179–184, 2006.
17. Ming-Der yang,"A Genetic Algorithm (GA) based automated classifier for remote sensing imagery", Can. J. Remote Sensing, No.3, Vol. 33, pp. 203-213,2007.
18. S Bandyopadhyay and U Maulik, "Nonparametric Genetic Clustering: Comparison of Validity Indices," IEEE Trans. Systems man and cyber., C, vol. 31, pp. 120-125, 2001.
19. S. Bandyopadhyay and U. Maulik, "An evolutionary technique based on K-Means algorithm for optimal clustering in RN," Information Sciences, vol. 146, no. 1–4, pp. 221–237, 2002.
20. Cadau E.G., Burini A, Putignano C, Goryl P, Gascon F." Multi-sensor rapid fire damage assessment over mediterranean area". 34th International Symposium on Remote Sensing of Environment; Sydney, Australia. 2011.
21. Rong-Rong Li, Yoram J. Kaufman, Wei Min Hao, J. Meghan Salmon, Bo-Cai Gao "A Technique for Detecting Burn Scars Using MODIS Data" IEEE transactions on geoscience and remote sensing, VOL. 42, 2004.
22. Zhang J, Wagner W, Prakash A, Mehl H, Voigt S. "Detecting coal fires using remote sensing techniques". Int J Remote Sens. 25:3193–3220, 2004.
23. Walker W.S., Stickler CM, Kellndorfer JM, Kirsch KM, Nepstad DC. 2010. Large-area classification and mapping of forest and land cover in the Brazilian Amazon: a

comparative analysis of ALOS/PALSAR and Landsat data sources. IEEE J Select Topics Appl Earth Observ Remote Sens. 3:594-604., 2010.

24. P. Mishra and D. singh,"Land cover classification of PALSAR images by knowledge based decision tree classifier and supervised classifiers based on SAR observables" Progress In Electromagnetics Research B, Vol. 30, 47–70, 2011.
25. Chang, Chein-I., and Hsuan Ren. "Linearly constrained minimum variance beamforming approach to target detection and classification for hyperspectral imagery." In Geoscience and Remote Sensing Symposium, 1999. IGARSS'99 Proceedings. IEEE 1999 International, vol. 2, pp. 1241-1243. IEEE, 1999.
26. Haertel V. F. and Shimabukuro Y. E., "Spectral linear mixing model in low spatial resolution image data," IEEE Transactions on Geoscience and Remote Sensing, vol. 43, no. 11, 2005, pp. 2555–2562.
27. Chang C. and Wang S., "Constrained band selection for hyperspectral imagery," IEEE Transactions on Geoscience and Remote Sensing, vol. 44, no. 6, 2006, pp. 1575–1585.
28. Chang C., Liu J., Chieu B., Ren H., Wang C., Lo C., Chung P., Yang C., and Ma D., "Generalized constrained energy minimization approach to subpixel target detection for multispectral imagery," Optical Engineering, vol. 39, no. 5, 2000, pp. 1275–1281.
29. Ren H. and Chang C., "Target-constrained interference-minimized approach to subpixel target detection for hyperspectral images," Optical Engineering, vol. 39, no. 12, 2000, pp. 3138–3145.
30. Ren H., Du Q., Chang C., and Jensen J. O., "Comparison between constrained energy minimization based approaches for hyperspectral imagery," IEEE Workshop on Advances in Techniques for Analysis of Remotely Sensed Data, 2003, pp. 244–248.
31. Settle J., "On constrained energy minimization and the partial unmixing of multispectral images," IEEE Transactions on Geoscience and Remote Sensing, vol. 40, no. 3, 2002, pp. 718–721.
32. Chang, Chein-I., and Daniel C. Heinz. "Constrained subpixel target detection for remotely sensed imagery." Geoscience and Remote Sensing, IEEE Transactions on 38, no. 3 (2000): 1144-1159.
33. Chang C. and Wang S., "Constrained band selection for hyperspectral imagery," IEEE Transactions on Geoscience and Remote Sensing, vol. 44, no. 6, 2006, pp. 1575–1585.

34. Gautam. R, "Study of dip techniques to detect hotspots with low resolution satellite data", Ph.D Thesis, Department of Electronics and communication Engineering, IIT Roorkee, India, 224p, 2008.
35. Mishra, Rakesh Kumar and Pandey, J. and Khalkho, Ajay and Singh, V.K. " Estimation of air pollution concentration over Jharia coalfield based on satellite imagery of atmospheric aerosol", International Journal of Geomatics and Geosciences, 2 (3). pp. 723-729. ISSN 0976-4380, 2012.
36. Gupta, R. P., and A. Prakash. "Cover: Reflectance aureoles associated with thermal anomalies due to subsurface mine fires in the Jharia coalfield, India." (1998): 2619-2622.
37. Goetz, A. F. H., Rock, B. N., and Rowan, L. C., 1983, Remote sensing for exploration: an overview, Economic Geology, 79, 573- 590.
38. Gupta, R. P., 1991, Remote Sensing Geology (Berlin-Heidelberg: Springer-Verlag).
39. Satterwhite, M. B., and Ponder, H. J., 1987, Spectral characteristics of selected soils and vegetation in Northern Nevada and their discrimination using band ratio techniques. Remote Sensing of Environment, 23, 155- 175.
40. Morton J., "Image Analysis, Classification and Change Detection in Remote Sensing: With Algorithms for ENVI/IDL", CRC Press, 2006.
41. John A. Richards and Xiuping Jia, "Remote Sensing Digital Image Analysis An Introduction", Springer, 2006.
42. Roy, "Introduction to Soft Computing: Neuro - Fuzzy and Genetic Algorithms", Pearson Education, 2013.
43. D. E. Goldberg, "Genetic Algorithms in Search, Optimization and Machine Learning", Addison-Wesley, 1989.
44. Sch¨olkopf, B., Smola, A., Williamson, R. C., & Bartlett, P."New support vector algorithms. Neural Computation," vol.12, 1207–1245, 2000.
45. Vapnik, V. N. 1995. The Nature of Statistical Learning Theory. (New York: Springer-Verlag).
46. Foody, M. G., and Mathur, A. 2004. A Relative Evaluation of Multiclass Image Classification by Support Vector Machines. IEEE Transactions on Geoscience and Remote Sensing, 42,1335– 1343.

47. Foody, M. G., and Mathur, A. 2004. Toward Intelligent Training of Supervised Image classifications: Directing Training Data Acquisition for SVM Classification. Remote Sensing of Environment, 93,107 - 117.
48. Christianini, N., and Shawe-Taylor, J. 2000. An introduction to support vector machines: and other kernel-based learning methods. (Cambridge and New York: Cambridge University Press).
49. Campbell, C. 2000. An Introduction to kernel Methods, Radial Basis Function Networks: Design and Applications. (Berlin: Springer Verlag).
50. Plaza A., Martínez P., Pérez R., and Plaza J., "A quantitative and comparative analysis of endmember extraction algorithms from hyperspectral data," IEEE Transactions on Geoscience and Remote Sensing, vol. 42, no. 3, 2004, pp. 650–663.
51. Plaza, Antonio, Pablo Martínez, Rosa Pérez, and Javier Plaza. "A quantitative and comparative analysis of endmember extraction algorithms from hyperspectral data." Geoscience and Remote Sensing, IEEE transactions on 42, no. 3 (2004): 650-663.
52. Boardman, Joseph W., Fred A. Kruse, and Robert O. Green. "Mapping target signatures via partial unmixing of AVIRIS data." (1995).
53. Chang C. and Plaza A., "A fast iterative algorithm for implementation of pixel purity index," IEEE Geoscience and Remote Sensing Letters, vol. 3, no. 1, 2006, pp. 63–67.
54. Harsanyi, Joseph C. Detection and Classification of Subpixel Spectrla Signatures in Hyperspectral Image Sequences. UMI, 1993.
55. Nielsen, Allan Aasbjerg. "Linear mixture models, full and partial unmixing in multi-and hyperspectral image data." IN PROCEEDINGS OF THE SCANDINAVIAN CONFERENCE ON IMAGE ANALYSIS, vol. 2, pp. 895-902. 1999.
56. Otsu, Nobuyuki. "An automatic threshold selection method based on discriminate and least squares criteria." Denshi Tsushin Gakkai Ronbunshi 63 (1979): 349-356.
57. Mantas Paulinas, Andrius Ušinskas "A survey of genetic algorithms applications for image enhancement and segmentation" information technology and control, Vol.36, No.3, ISSN 1392 – 124X, 2007.
58. Yoo, Terry S. Insight into images: principles and practice for segmentation, registration, and image analysis. AK Peters Ltd, 2004.

59. Prakash A., "Remote sensing - GIS based geoenvironmental studies in Jharia Coalfield, India, with special reference of coalmine fires," Ph.D. Thesis, Department of Earth Sciences, UOR, Roorkee, India, 1996, 194 p.